MAGDAS/CPMN PROJECT FOR LITHO-SPACE WEATHER DURING IHY/ISWI (2007-2012)
MAGDAS/CPMN ПРОЕКТ ДЛЯ ЛИТОСФЕРНО-КОСМИЧЕСКОЙ ПОГОДЫ ВО ВРЕМЯ IHY/ISWI (2007-2012)

K.Yumoto [1] and the MAGDAS/CPMN Group

[1] Space Environment Research Center, Kyushu University,

Мы представляем систему сбора магнитных данных в реальном времени Тихоокеанской магнитометрической сети, т.е. MAGDAS/CPMN, для изучения космической погоды и прикладного использования, которая развернута во время Международного Гелиофизического года (МГГ 2007-2009). Используя эту систему, мы проводим мониторинг в реальном времени и моделирование (1) глобальной трехмерной токовой системы, (2) плотности плазмы, и (3)процесс проникновения полярных электрических полей в экваториальную ионосферу, для понимания системы солнечно-земного взаимодействия и изменения космической плазмы. В настоящем докладе мы рассмотрим полученные недавно результаты в течение МГГ и кратко состояние координированных наблюдений во время Международного инициативного периода по космической погоде(ISWI) (2010-2012).

1. Introduction

In 1957–58, more than 66,000 scientists and engineers from 67 nations participated in the International Geophysical Year (IGY). Fifty years on, the International Heliophysical Year (IHY) again drew scientists and engineers from around the globe in a coordinated campaign to observe the heliosphere and its effects on planet Earth. For the benefit of scientists and engineers from developing nations, the United Nations Office for Outer Space Affairs, through the United Nations Basic Space Science Initiative (UNBSSI), assisted scientists and engineers from all over the world in participating in the activities of IHY 2007–2009 (United Nations, 2006).

The IHY was an extensive international program undertaken to study the universal physical processes in the heliospace in order to gain a better understanding of the Sun-heliosphere system (cf. Yumoto et al., 2009b). Particular attention was paid to the neutral and ionized matter in the heliospace from the Sun to the atmospheres of Earth and the other planets and throughout the interplanetary medium. The IHY continued the legacy of the IGY by extending the geophysical studies performed 50 years ago to the combined system of the Sun and the planets. IHY also extended the physical realm from geospace to heliospace, recognizing the enormous progress made over the past 50 years. There were four key elements of IHY: 1) science (coordinated investigation programs conducted as campaigns to investigate specific scientific questions, 2) instrument development (the IHY/UNBSS program), 3) public outreach (to communicate the beauty, relevance and significance of space science to the general public and students), and 4) the IGY Gold Club program (to identify and honor the scientists who participated in the IGY program).

In June of 2006, the Science Council of Japan formally recognized the STPP (Solar Terrestrial Physics Program) subcommittee for International Affairs, Committee on Earth and Planetary Sciences, as the IHY National Steering Committee for Japan. The committee was chaired by Kiyohumi Yumoto and promoted the followings (see the details of Yumoto et al., 2009b)

(1) satellite missions launched or to be launched by Japan,
(2) international network observations,
(3) public outreach,
(4) international and domestic workshops, and
(5) nomination of Japanese scientists as IGY Gold Club members.

On the other hand, one purpose of the Solar Terrestrial Physics (STP) research in the twenty-first century is to support human activities from an aspect of fundamental study. The scientific new aim for the STP society is a creation of new physics; (1) couplings of the complex and composite systems and (2) multi-scale couplings in the Sun-Earth system. The goals for the attainment of the purpose are to construct Network Stations for observations and Modeling Stations for simulation/ empirical modeling. In order to understand the Sun-Earth system and its effects to human lives, the international LWS (Living With Star) and CAWSES (Climate And Weather of Sun-Earth System) programs started from 2004. The International Heliophysical Year (IHY) program also started in 2007.

For space weather study on the complexity in the Sun-Earth system, the Space Environment Research Center (SERC), Kyushu University started to construct a new ground-based magnetometer network, in cooperation with about 30 organizations around the world from 2004 (Yumoto et al., 2006 and 2007, Otadoy, et al., 2009). The SERC is conducting the MAGDAS (MAGnetic Data Acqusition System) observations along 210° magnetic meridian (MM) and along the magnetic equator in the CPMN (Circum-pan Pacific Magnetometer Network) region (Yumoto et al., 2009d and 2009e), and the FM-CW (Frequency Modulated Continuous Wave) radar observations along the 210°MM (Ikeda et al., 2008, 2010a and b, Yumoto et al., 2009c), in order to understand dynamics of plasmaspheric changes during space storms, responses of magnetosphere-ionosphere-thermosphere to various solar wind changes, and penetration mechanisms of DP2-ULF range disturbances from the solar wind region into the equatorial ionosphere. From 2008, MAGDAS-II magnetometers have been installed along the 96° magnetic meridian in Africa to understand the longitudinal dependence of long-, short-term Sq variations, DP-2, sc, si, and of Ultra Low Frequency (ULF) waves (Maeda G. et al., 2009, Rabiu et al., 2009a and 2009b). On the other hand, electromagnetic phenomena, e.g., ULF, ELF and VLF waves are recognized as useful diagnostic probes of the solar wind-magnetosphere-ionosphere-atmosphere coupled system for space weather studies. These waves convey information about the dynamics and morphology of the coupled system.

In the present review paper, at the first we will introduce our real-time data acquisition and analysis systems of MAGDAS/CPMN and MAGDAS-II, and scientific results obtained by these systems during the IHY (2007-2009); (1) the global 3-dimensional current system to understand the electromagnetic coupling of high-latitude, Sq, and EEJ current systems and their long-term variations, and (2) global characteristics of ULF waves (Pc 3, 4, and 5, and Pi 2) in geo-space to know magnetospheric environment changes during storms and substorms. In the second, we will show the FM-CW radar systems along the 210°MM to deduce electric field variations from the ionospheric plasma Doppler velocity. From 24hr measurement of the ionospheric drift velocity with 3 and/or 10-sec sampling rate by the FM-CW radar observation, (3) we can understand how the polar electric field penetrates into the equatorial ionosphere.

2. MAGDAS/CPMN network

2.1. Motivation

The MAGnetic Data Acquisition System (MAGDAS) group at the Space Environment Research Center (SERC) of Kyushu University, Fukuoka, Japan seeks to deploy around the world in a strategic fashion a new generation of tri-axial fluxgate magnetometers (called MAGDAS) that transfer the digitized data to a central SERC server in real-time for space weather study and application during the IHY period (2007–2009). The strategy is to put the magnetometers in well-defined ‘‘bands’’ on the globe that are useful for scientific exploration.

The first band is the strip that goes north and south of Japan—up to Siberia and down to the Antarctic. In our geo-space field, this north–south band is also known as the ‘‘210 Magnetic Meridian’’ and became famous in this field of geospace research (Yumoto and the 210MM Magnetic Observation Group, 1996a). After the international solar terrestrial energy program (STEP) period (1990–1997), 1-sec magnetic field data from coordinated ground-based network stations made it possible to (1) study magnetospheric processes by distinguishing between temporal changes and spatial variations in the phenomena, (2) clarify global structures and propagation characteristics of magnetospheric variations from polar to equatorial latitudes, and (3) understand the global generation mechanisms of various solar-terrestrial phenomena (Yumoto and the CPMN group, 2001). In this north–south band, the average spacing of magnetometers is 500 km. The most northern magnetometer is at Cape Schmidt in northern Russia. The most southern magneto- meter is located at Davis Station of AAD (Australian Antarctic Division).

The second band is the geomagnetic ‘‘dip’’ equator. SERC has completed most of the installations along this band (Yumoto and the MAGDAS Group, 2007). One big gap, however, is the Pacific Ocean; we are still searching for a suitable island in the middle of it. The third band runs up and down the continent of Africa; SERC has already

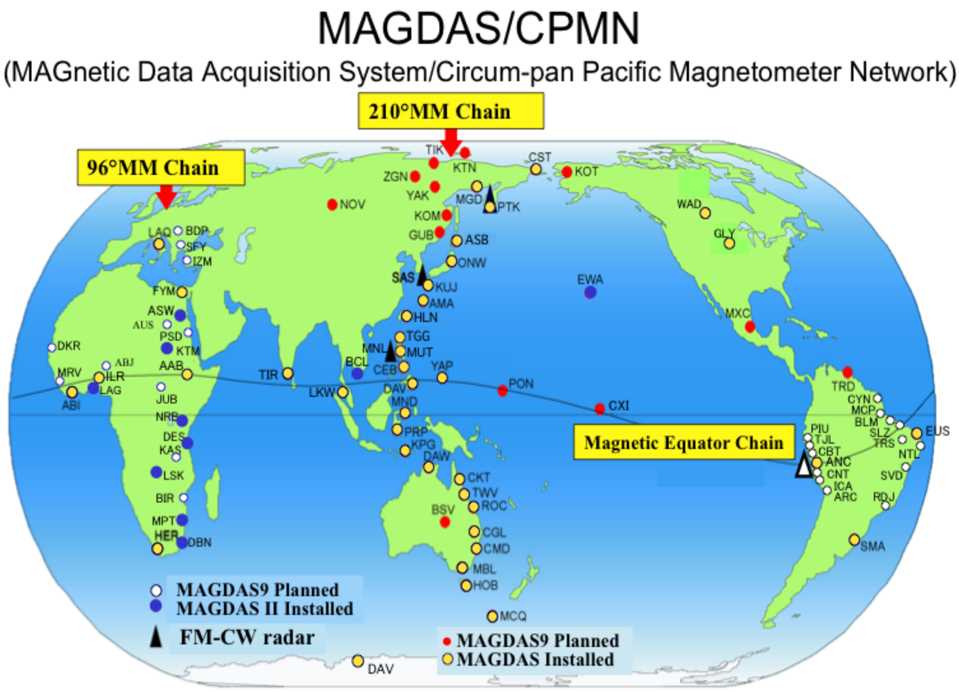

Fig. 1. The non-blue dots are installed or soon-to-be installed MAGDAS magnetometers. They are concentrated in four bands. The black triangles are SERC FM-CW radars (for ground-based observation of the ionosphere). The blue dots are MAGDAS II magnetometers but whose discussion go beyond the scope of this paper.

completed the installation from South Africa at the Hermanus Magnetic Observatory, through Egypt near Cairo, to Italy. The fourth band runs up and down the Americas; SERC installed several magnetometers in North and South America. Figure 1 is a map of MAGDAS and MAGDAS II stations.

With scientifically significant real-time data arriving at SERC from over 50 MAGDAS and MAGDAS II magnetometers (and identically calibrated magnetometers, and which are sensitive down to the nT level), SERC seeks to conduct socially beneficial space weather forecasting. SERC also has a policy to establish an important new research tool for the geospace community: Our EE-index (EDst, EU, and EL) in 3.3. sub-session is being proposed to monitor transient and long-term variations of the Equatorial Electrojet by using MAGDAS/CPMN real-time data (Uozumi et al. 2008).

2.2. Description of MAGDAS

The MAGDAS system is divided into two portions: MAGDAS-A and MAGDAS-B. MAGDAS-A is a real-time magnetometer unit installed at Circum-pan Pacific Magnetometer Network (CPMN) stations, while MAGDAS-B is a data acquisition and monitoring system installed at SERC. MAGDAS-A as a whole consists of a sensor unit, data logger/transfer units, and power supply (Fig. 2). The sensor unit of MAGDAS-A system consists of tri-axial ring-core sensors, two tilt-meters and a thermometer (Fig. 3). Magnetic field digital data (H+dH, D+dD,

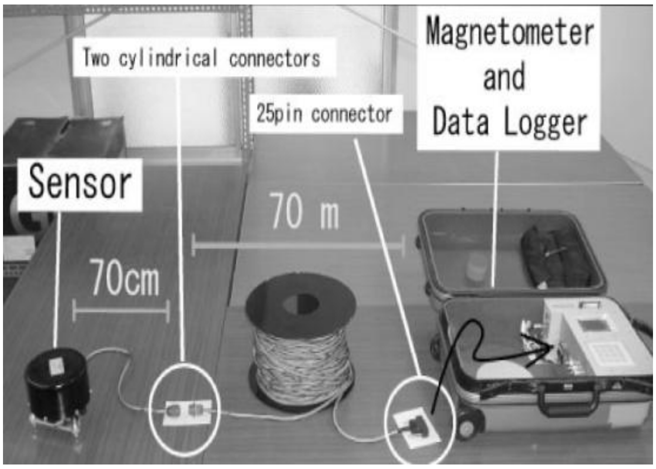

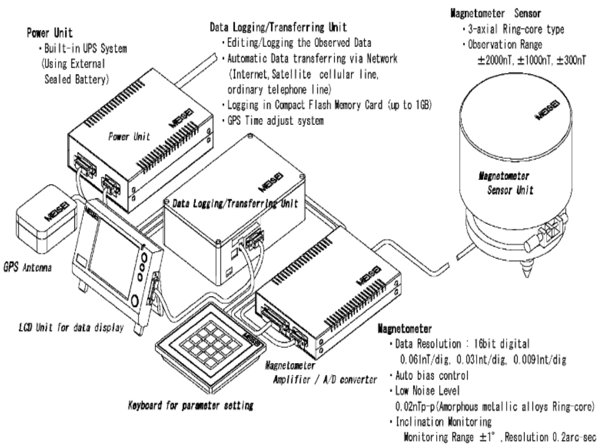

Fig. 2a. This is photo of MAGDAS Unit 08 (taken at SERC by G. Maeda). Easily visible are the: (1) grey AC power cord, (2) round and black sensor with its 1-meter cable, (3) the 70-meter cable reel, (4) main case (modified travelers suitcase), and (5) GPS antenna with 25-meter cord. The output of the sensor is analog. The electronics inside the main case converts this analog data into digital data, which is sent to SERC via the Internet and is stored locally on a CF card for redundancy.

Fig. 2b. The component of MAGDAS/CPMN magnetometer system for real-time data acquisition.

Z+dZ, F+dF) are obtained with the sampling rate of 1/16 s, and then the 1-sec averaged data are transferred from each overseas station to SERC, Japan, in real time (Yumoto and MAGDAS Group 2006). To facilitate installation in just about any spot on the globe, MAGDAS-A was specially designed to be portable (hand-carried suitcase) and lightweight (just 15 kg). Visible in Fig. 2 are all vital components. The required power is just 20 W. The best way for SERC to get the data in real-time from this instrument (we have found out from sheer experience) is via the Internet. (The machine was designed with other options.) However, for redundancy, the data is stored onto a high-capacity compact flash semiconductor memory card (1.0 or 0.5 GB). The cord for the GPS antenna is about 25 m. This antenna is usually placed on the roof of the building in which the main case resides. The sensor is placed in a separate structure to be away from building-related noise (e.g., noise from electric motors). To allow ample separation, the sensor cable is 70 m in length. In Fig. 2a, the cable is

Fig. 3 This is the MAGDAS sensor with the round and black cover removed. The two brass-colored devices are precision tiltmeters. The rest form a tri-axial fluxgate magnetometer. This photo was taken at SERC by G. Maeda last year when the magnetometer had to be repaired.

wound up on the reel (to allow for delivery from SERC to the final site overseas). The component of MAGDAS is described in Fig. 2b.

The sensor's analog data is continuously digitized. The ambient magnetic fields, expressed by horizontal (H)-, declination (D)-, and vertical (Z)-components, are digitized by using the field-canceling coils for the dynamic range of ±64,000nT/16bit. The magnetic variations (dH, dD, dZ) subtracted from the ambient field components (H, D, Z) are further digitized by a 16-bit A/D converter. Two observation ranges of ±2,000 nT and ±1,000 nT can be selected for high- and low-latitude stations, respectively. The total field (F + dF) is estimated from the H + dH, D + dD, and Z + dZ components. The resolution of MAGDAS data is 0.061nT/LSB and 0.031nT/LSB for the ±2,000 nT range and ±1,000 nT range, respectively. About 1.5 MB of data is generated each day as a result. Data from all MAGDAS units flow into a central server at SERC. This raw data must be processed to become scientifically useful. All the processing takes place here at SERC. This data can be accessed by anyone via the Web (http://magdas.serc.kyushu-u.ac.jp/), with some conditions attached.

Installation of the sensor (see Fig. 3) is complicated because it must be carefully aligned in three ways. First, it must be pointed exactly north with precision threading. Second, it must be perfectly level (resulting in two orthogonal adjustments). This levelness is achieved with the precision threading of a tripod base. The long-term inclinations (I) of the sensor axes can be measured by two tilt-meters with resolution of 0.2 arc-sec. The temperature (T) inside the sensor unit is also measured. GPS signals are received to ''keep correct'' the standard time inside the data logger/transfer unit. These data are recorded on to the compact flash memory card as data backup.

2.3. Calibration for temperature drift of MAGDAS

For quantitative analysis of various geomagnetic phenomena, which are observed in wide longitudinal and latitudinal area (e.g., as shown in Fig. 1), it is necessary to analyze precise and standardized magnetic field data. For instance, the stability of the base magnetic variation and the absolute sensitivity are very important for the study of the Equatorial Electrojet (EEJ) and Counter Electrojet (CEJ) (e.g., Uozumi et al., 2008), Sq (e.g., Yamazaki et al., 2009b), SC/SI (e.g., Kitamura et al., 1998, Yumoto et al., 1996b and 2009c) and ULF (e.g., Yumoto et al., 1996 and 20001, Uozumi et al., 2004 and 2009b; Abe et al., 2006, Tokunaga et al., 2007). It is also indispensable to grasp the accuracy of the data to be analyzed, because this matter critically limits the quantitative validity or reliability of analyses. Thus, Uozumi et al. (2009a) have investigated and developed a calibration technique for the MAGDAS/CPMN ground magnetic field data, which is obtained by MAGDAS fluxgate magnetometer made by the Meisei Electric Co., Ltd. They have also evaluated quantitatively the suitability of the method, and estimated the expected accuracy of the calibrated MAGDAS magnetic data. The result provides fundamental information on the accuracy limit of MAGDAS magnetic data, and would be

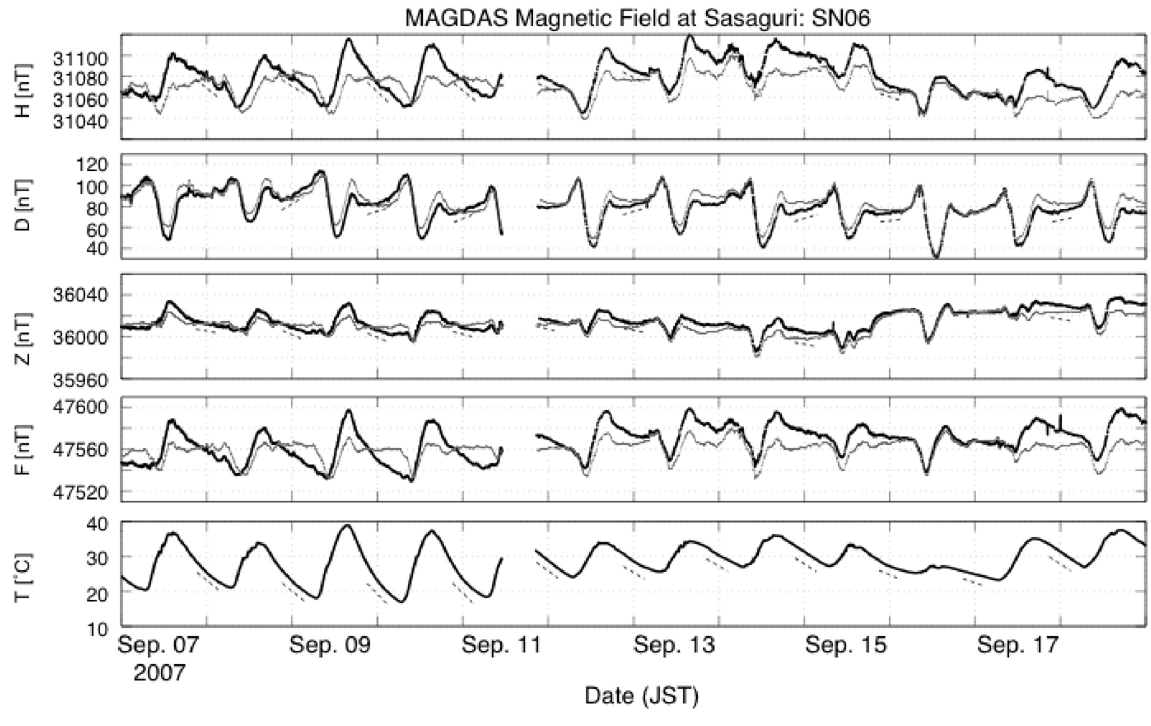

Fig. 4. Thick curves plot the MAGDAS raw (original) magnetic field (*H*, *D*, *Z*, *F*) and the sensor-head temperature (*T*) observed at Sasaguri during the period of Sep. 7-18, 2007 (JST). Thin curves plot corrected magnetic field data of each component. Dashed lines indicate the trend of the variation for each component around midnight.

standard of the reliability on all geophysical results derived by the MAGDAS data.

The thick curves in Figure 4 plot the raw (original) magnetic field (*H*, *D*, *Z*, *F*) and the sensor-head temperature (*T*), which was observed at Sasaguri station (GGLAT=33.64°, GGLON=130.51°) during the period of September 7-18, 2007 in JST (UT+9hour). Sasaguri Station is the observatory for experimental tests and calibration of MAGDAS/CPMN magnetometer system, and is located in the suburban area near SERC (about 8km distance). As shown in Fig. 4, nighttime variations of the *H*, *D*, *Z* and *F* tend to increase/decrease as *T* decreases. Dashed lines indicate the trend of the variation for each component around midnight. The thin curves in Fig. 4 represent the corrected data. It is well known that the base nighttime magnetic variation traces close to straight line for the first approximation, except the time of active geomagnetic situation such as magnetic storm (e.g., Matsushita and Campbell, 1967). Thus magnetic variation, which is correlated with temperature variation, is considered as not geomagnetic phenomena but artificial variation. The artificial component of the magnetic variation is well correlated with the temperature variation. Thus, they assumed that the artificial component of the magnetic variation is proportional to the temperature variation. They called this type of magnetic variation as “temperature drift”. Based on this assumption, they developed a correction technique of the MAGDAS magnetic field data. Magnetic field variation, which was observed by MAGDAS magnetometer of the serial number 6 (SN06) during the period of September 7-18, 2007, was used as test data for developing the correction method. The detail of the correction method is explained in the paper of Uozumi et al. (2009a). The corrected data represent that the nighttime variation traced almost a constant value. On the other hand in daytime, daily magnetic variation, so-called Sq (solar quiet) variation is usually observed. The real geomagnetic variation should be estimated by correcting the original data. They confirmed that the raw magnetic field data can be corrected by subtracting the temperature drift component, which will be estimated by the derived factor. Theye evaluated the quantitative validity of the correction method. The correction method is concluded to be suitable for practical use.

3. Scientific objectives and recent MAGDAS results

In order to establish the space weather studies, we have to clarify dynamics of geospace plasma changes during magnetic storms and auroral substorms, the electro-magnetic response of iono-magnetosphere to various solar wind changes, and the penetration and propagation mechanisms of DP2-ULF range disturbances from the solar wind region into the equatorial ionosphere. Figure 5 shows one example of amplitude-time records of 3-component ordinary (upper) and induction-type (bottom) magnetograms observed at the Kujyu station in Oita, Japan, during 24 hrs. The ordinary data (i.e. MAGDAS data (1)) can be used for studies of long-term variations, e.g. magnetic storm, auroral substorms, Sq, etc., while the induction-type data (i.e. MAGDAS data (2)) will be useful for studies of ULF waves, transient and impulsive phenomena. By using these new MAGDAS data, we can conduct a real-time monitoring and modeling of (1) the global 3-dimensional current system and (2) the ambient plasma density for understanding the electromagnetic and plasma environment changes in the geospace.

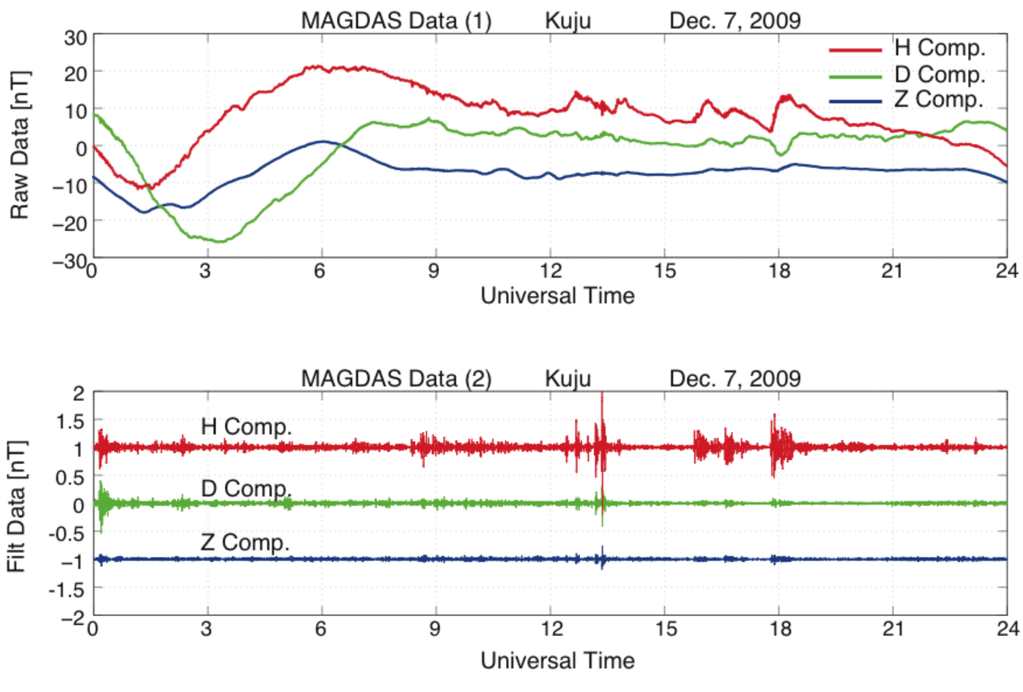

Fig. 5. An example of amplitude-time records of ordinary (upper; MAGDAS data (1)) and induction-typ.

3.1. Imaging of global 3-D current system

The left panel of Figure 6 indicates the ionospheric equivalent current pattern obtained from the CPMN stations along the 210°magnetic meridian during a northern summer. Each ionospheric current vector was estimated by the horizontal magnetic fields observed at each CPMN station at every hour. We will make the ionospheric equivalent current pattern every day using the MAGDAS data (1) as shown in Fig. 5. The right panel of Fig. 6 shows the global 3-dimensional currents and electric potential, with the currents illustrated by ribbons and the potential with + and – (Richmond and Thayer, 2000). At high latitudes the ionospheric currents are joined with **f**ield-**a**ligned **c**urrents (FAC) from the solar wind region into the magnetosphere, and the electro-dynamics is dominated by the influences of solar wind-magnetosphere interaction processes. The total current flows is of the order of 10^7 A. On the other hand, the ionospheric current at middle and low latitudes is generated by the ionospheric wind dynamo, which produces global current vortices on the dayside ionosphere, i.e., counterclockwise in the northern hemisphere and clockwise in the southern hemisphere. The total current flow in each vortex is order of 10^5 A.

There are strong electric fields at high latitudes, on the order of several tens of millivolts per meter or more depending on the magnetic activity. At middle and low latitudes electric fields are considerably smaller, typically a few millivolts per meter during magnetically quiet periods. During magnetic active periods the part of strong electric fields at high latitude can penetrate into middle and low latitudes, and then the global ionospheric current pattern must be re-organized strongly. In reality the current and electric fields at all latitudes are coupled, although those at high, and middle and low latitudes have been often considered separately. By using the MAGDAS ionospheric current pattern as shown in the left panel of Figure 6, the global electromagnetic coupling processes at all latitudes will be clarified during the ISWI period (2010-2012).

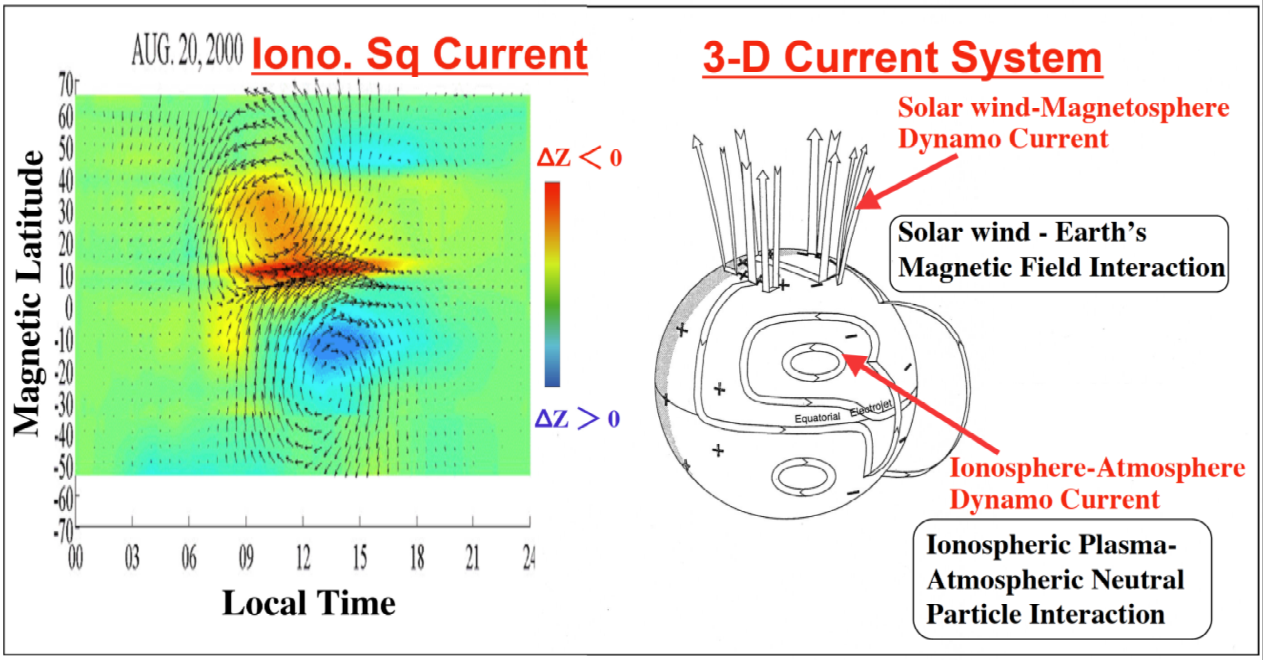

Fig. 6. (Left) The ionospheric equivalent current pattern obtained from the MAGDAS/CPMN data. (Right) Global 3-dimensional current system cased by magnetospheric field-aligned currents at high latitude and the ionospheric dynamo at middle and low latitudes.

Figure 7a shows equivalent ionospheric current patterns obtained from the MAGDAS Data (1) on September 25, 2005 (Kohta et al., 2005). The vertical axis indicates magnetic latitudes of the MAGDAS stations, and the horizontal axis is the local time of the 210° magnetic meridian stations. The arrows indicate the current vectors obtained from the H and D components, and the color code indicates the negative and positive magnetic Z component. The equatorial electrojet can be seen at the dayside dip equator. There are twin vortices of Sq current, i.e., counter-clockwise and clockwise in the northern and southern hemisphere, respectively. The centers of Sq current patterns are sometime not consistent with the maximum and minimum points of the Z component. Figure 7b is one example of Sq equivalent current pattern obtained by the CPMN data on July 15, 2000, during a disturbed day. The vertical axis indicates geographic latitudes of the CPMN stations, and the horizontal axis is the local time of the 210° magnetic meridian stations. A clear Sq current vortex, equatorial electrojet, auroral electrojet, and ring current patterns can be identified in the figure. It is newly found a current flowing from the northern hemisphere into the southern hemisphere around 06 hr local time during magnetic storm.

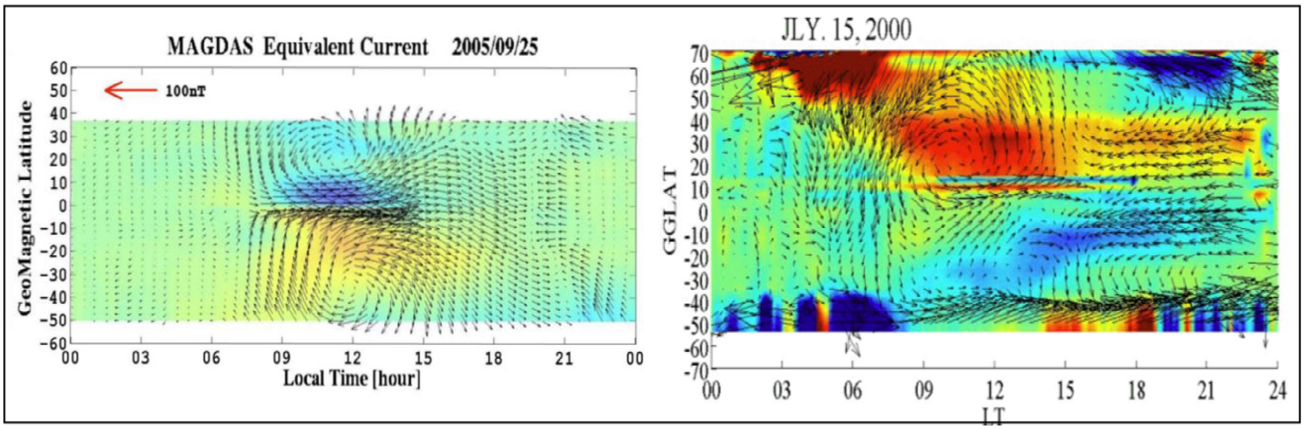

Fig. 7a and 7b. MAGDAS Sq current pattern on September 5, 2005 during magnetic quiet day (left), while CPMN Sq current pattern on July 15, 2000 during magnetic disturbed day (right) (Kohta et al., 2005).

3.2. Annual and semi-annual Sq current variations

Yamazaki et al. (2009b) analyzed ground magnetometer data for the 10 International Quiet Days during 1996-2007. The data were obtained from 19 stations along 210° Magnetic Meridian (MM) of the Circum-pan Pacific Magnetometer Network (CPMN) covering both the northern and southern hemispheres. From the daily variations of the geomagnetic field, we deduced the latitude-local time (LAT, LT) diagram of the equivalent Sq current system, which can be regarded as the superposition of the following three current systems: **Sq0**, **Sq1** and **Sq2** current systems. The **Sq0**, **Sq1** and **Sq2** current systems are equivalent current systems for the yearly average, annual variation and semi-annual variation of the Sq field, respectively. We have examined temporal and spatial features of these current systems. The principal features are as follows: (1) the total current intensity of the **Sq1** and **Sq2** current systems are about 35% and 15% of the **Sq0** current system, respectively. (2) the **Sq0** and **Sq2** current systems have a dayside vortex in each hemisphere, while the **Sq1** cur rent system has a single vortex centered at the equatorial region in the morning sector (~ 10 LT).

They analyzed hourly data of the daily variation of the geomagnetic field components ΔH and ΔD, where the Δ symbol represents the deviation of the geomagnetic field value from the zero level which is defined as the mean of the nighttime values (i.e., the values at 0000, 0100, 0200, 2200 and 2300 L.T.). The data of 10 International Quiet Days during 1996-2007 (as given by German Research Center for Geosciences (GFZ)) were selected. As is often pointed out, the International Quiet Days are not necessarily 'quiet' days but are just 'quietest' days for each month [e.g., Hibberd, 1981]. Consequently, the data for the International Quiet Days sometimes include severe effects from the magnetospheric and auroral activity, which can make irregular variations comparable to or larger than Sq variation range. Therefore, any visually-disturbed days which include irregularity obviously larger than Sq variation range were eliminated. The period of the analysis (i.e., 1996-2007) covers almost one solar cycle. The solar activity is known to control amplitudes of the Sq variation (ΔH, ΔD and ΔZ) [Rastogi et al., 1994]. Therefore, in order to reduce the solar-activity effect on the Sq amplitudes (ΔH and ΔD), the selected quiet days were divided into two levels of the solar activity (i.e., "high" and "low") based on the daily F10.7 solar flux data. They note that our distinction between "high" and "low" solar activity does not depend on the time of solar cycle. The data with $150 \leq$ F10.7 < 250 were classified as the data for the "high" solar activity period. On the other hand, the data with $50 \leq$ F10.7 < 150 were classified as the data for the "low" solar activity period. ΔH and ΔD are analyzed as a function of station latitude Φ, day of year d, local time LT and solar activity SA ("high" or "low"), i.e., ΔH(Φ, d,LT, SA) and ΔD(Φ, d,LT, SA), respectively. For a given Φ, LT and SA, ΔH(d) is represented by the sum of the following three components, namely, stationary component (ΔH0), annual component (ΔH1) and semi-annual component (ΔH2) as follows:

$$\Delta H(d) \sim \Sigma \Delta Hi(d) = \Delta H0 + \Delta H1(d) + \Delta H2(d) \qquad (1)$$

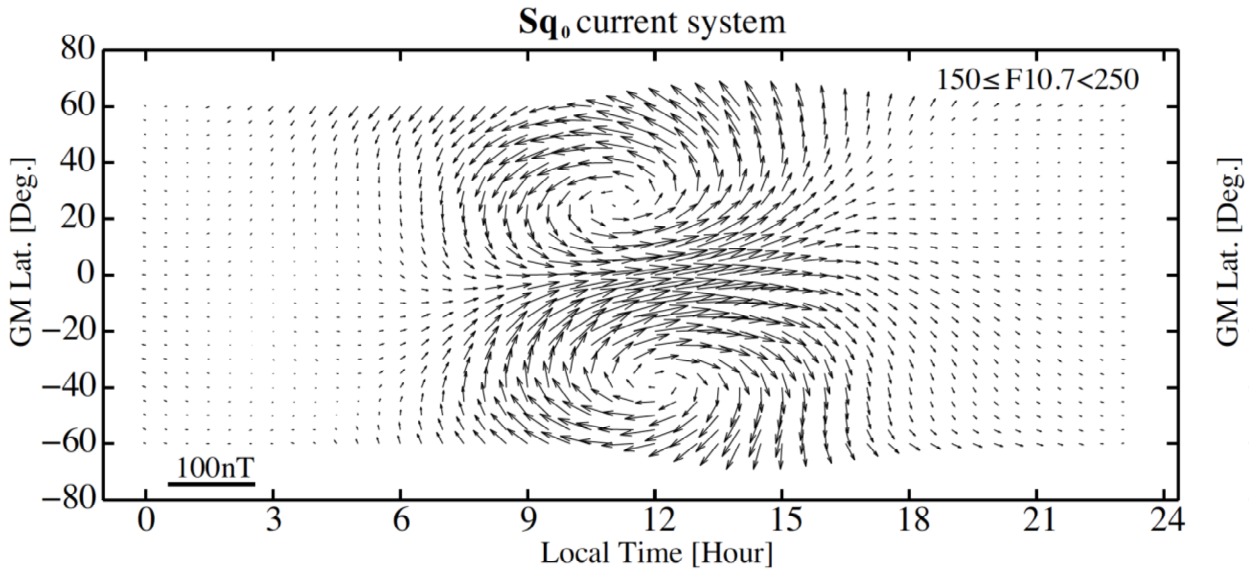

Fig. 8. The LAT-LT diagram of the Sq0 current system (i.e., the equivalent current system for the yearly average of the Sq field) during the ”high” solar activity period. See the section 2 of Yamazaki et al. (2009) for the construction details of the LAT-LT diagram.

In the same manner, ΔD(d) is represented.

Figure 8 shows the LAT-LT diagram of the **Sq**0 current system (i.e., the equivalent current system for the yearly average of the Sq field) for the ”high” solar activity period. It is seen that the **Sq**0 current system is composed of two dayside vortices with clockwise direction in the southern hemisphere and counter-clockwise in the northern hemisphere. Figures 9 and 10 show LAT-LT diagrams of the **Sq**1 and **Sq**2 current systems (i.e., the equivalent current systems for the annual and semi-annual variations of the Sq field), respectively, for different seasons of the ”high” solar activity periods. This is the first time that the equivalent current systems of the annual and semi-annual Sq variations are derived. The morphology of the **Sq**1 current system is characterized by a single vortex pattern centered at the equatorial region in the morning sector (~ 10 L.T.), on the other hand, the **Sq**2 current system is composed of two dayside vortices like the **Sq**0 current system.

They compared the yearly-averaged total current intensities among the **Sq**0, **Sq**1 and **Sq**2 current systems. For each current system, the total current intensities from DOY = 1 to DOY = 365 was calculated and were averaged. It was found that the yearly-averaged total current intensity of the **Sq**0 current system is the largest of the three. The ratio of the yearly-averaged total current intensity of the **Sq**1 current system to that of the **Sq**0

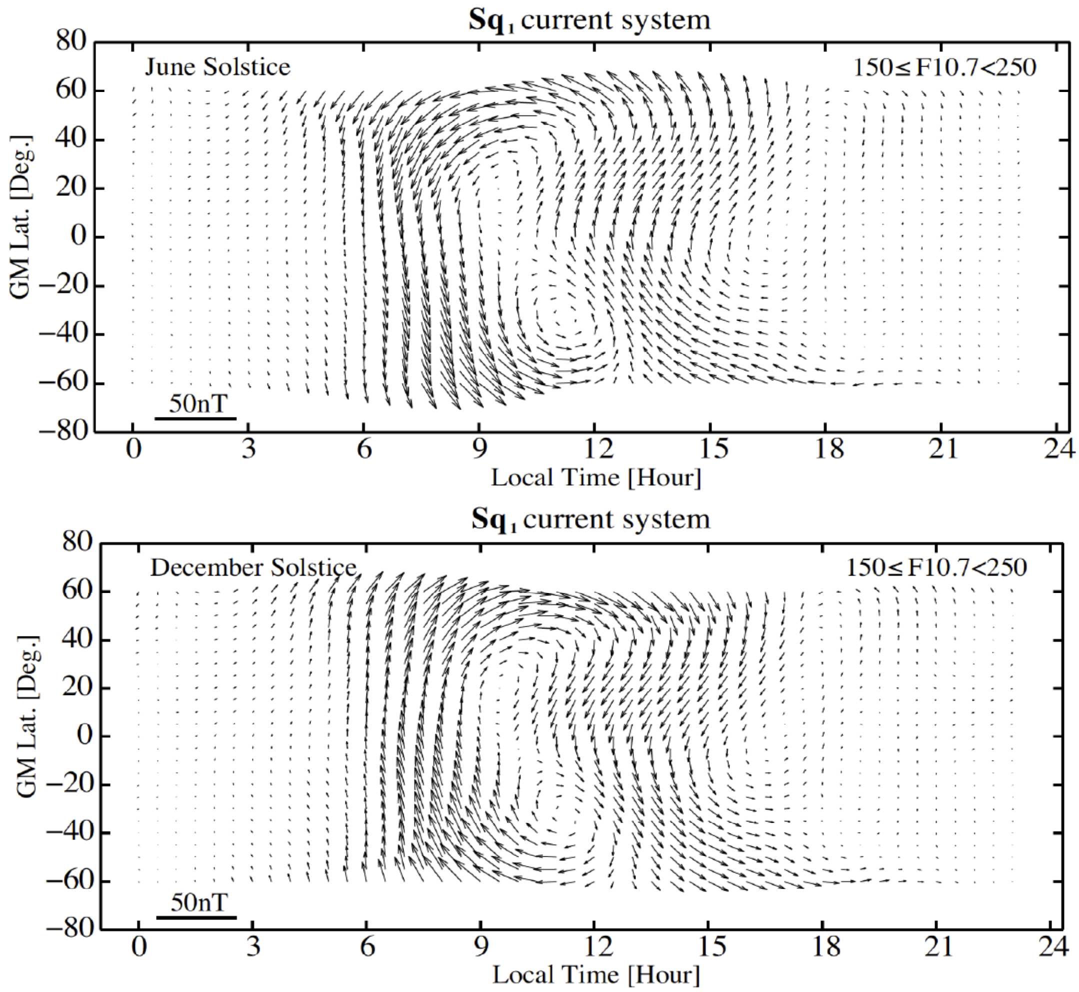

Fig. 9. The LAT-LT diagram of the Sq1 current system (i.e., the equivalent current system for the annual variation of the Sq field) for March equinox (D.O.Y. = 80, upper), and December solstice (D.O.Y. = 355, lower) during the ”high” solar activity period.

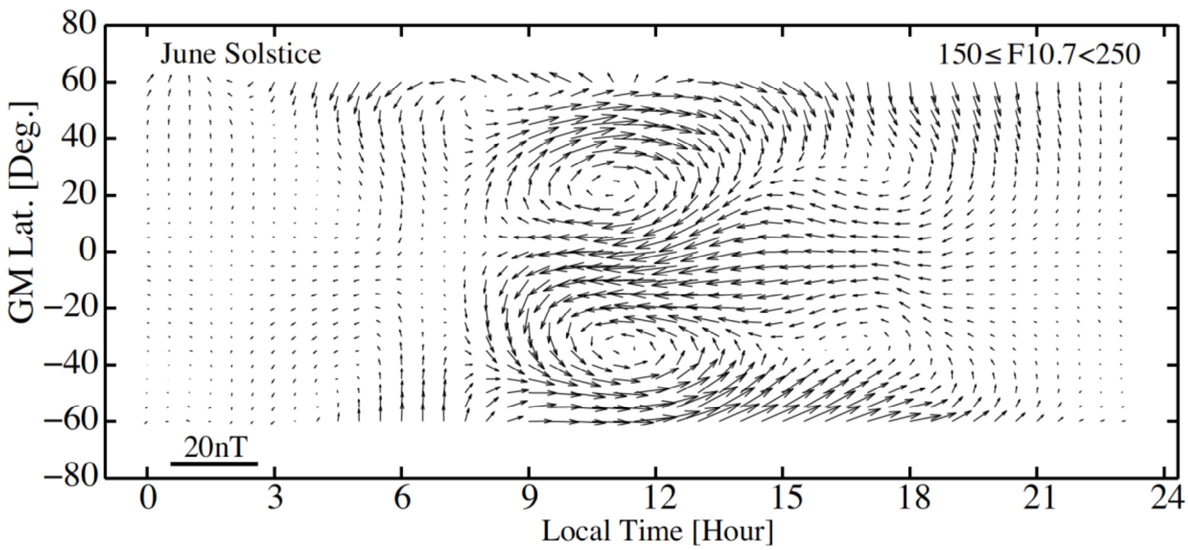

Fig. 10. The LAT-LT diagram of the Sq2 current system (i.e., the equivalent current system for the semi-annual variation of the Sq field) for June solstice (D.O.Y. = 172), during the ”high” solar activity period.

current system (**Sq1**/**Sq0**) is 0.31 for the ”high” solar activity period and 0.38 for the ”low” solar activity period On the other hand, the **Sq2**/**Sq0** is 0.15 and 0.16 for the ”high” and ”low” solar activity periods, respectively. They also examined phases of the **Sq**1 and **Sq**2 current systems. The phase is given by the day number d of the first peak in the total current intensity of the **Sq**1 and **Sq**2 current systems. The phase of the **Sq**1 current system appears on d = 186 (July 5) and d = 185 (July 4) for the ”high” and ”low” solar activity periods, respectively, which are about 10 days after the June solstice (June 21). On the other hand, the phase of the **Sq**2 current system appears near the March equinox (March 21) on d = 87 (March 28) and d = 83 (March 24) for the ”high” and ”low” solar activity periods, respectively.

3.3. A new EE-index and its long-term variation

A new index, EE-index (EDst, EU, and EL), is proposed by Uozumi et al. (2008) to monitor temporal and long-term variations of the equatorial electrojet by using theMAGDAS/CPMN real-time data. The mean value of the H component magnetic variations observed at the nightside (LT = 18–06) MAGDAS/CPMN stations along the magnetic equatorial region is found to show variations similar to those of Dst; we defined this quantity as EDst. The EDst can be used as a proxy of Dst for the real-time and long-term geospace monitoring. By subtracting EDst from the H component data of each equatorial station, it is possible to extract the Equatorial Electrojet and Counter Electrojet components, which are defined as EU and EL, respectively.

Figure 11a shows a superposed plot of the relative magnetic variation of the H component data ERS(m) (definition given just below) obtained for 1 month (Dec. 1–31, 2006), at the MAGDAS equatorial stations: Addis Ababa (AAB: Dip Lat. = 0.57◦; GMLON = 110.47◦), Davao (DAV: −0.65◦; 196.54◦), Ancon (ANC: 0.74◦; 354.33◦) and Eusebio (EUS: −7.03◦; 34.21◦). The “S” and “m” in “ERS(m)” refer to a station and a point of time in UT, respectively. In order to obtain ERS(m), the median value of the H component data, which is determined for the period from the start time of the observation to the end time of ERS(m), was subtracted from the original magnetic data for each station. It was found (not shown) that the median value, which was calculated from all the data in the abovestated interval, could estimate the non-disturbed nighttime ambient level. The determination by shorter-period data might cause some jumps in the base level among different

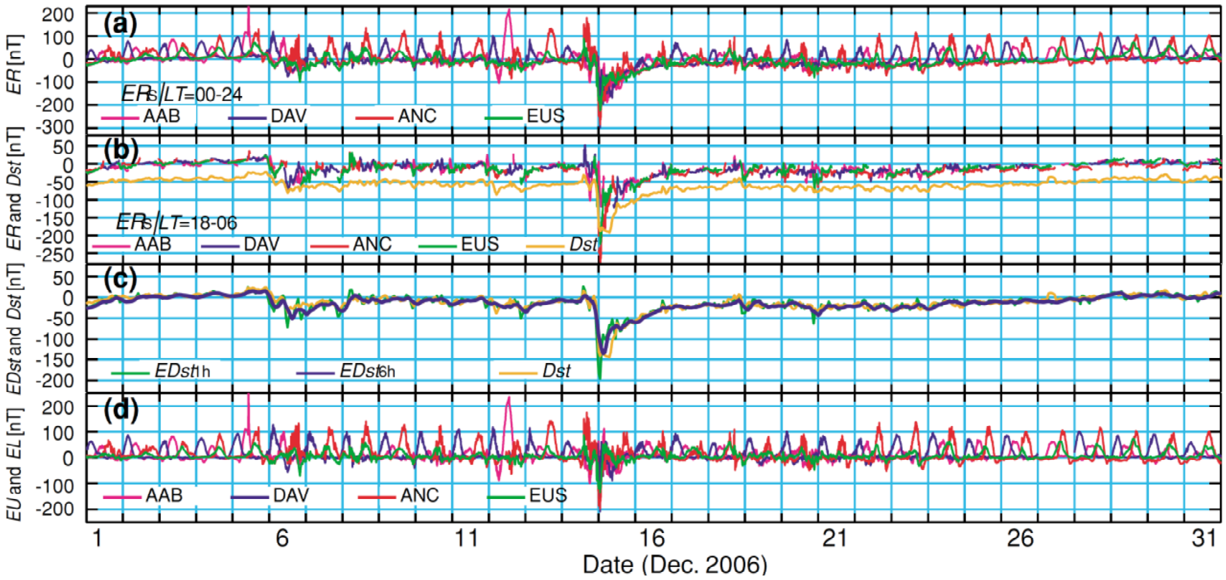

Fig. 11. One month plot of (a) relative magnetic variation of the H component (ERS |LT=00–24) observed by MAGDAS/CPMN equatorial network stations, (b) relative night time (LT=18–06) variation of the H component (ERS |LT=18–06) and the real-time Dst, (c) EDst1h, EDst6h and the real-time Dst, and (d) EU and EL for MAGDAS/CPMN equatorial network stations, during one month of December 2006.

periods (it might occur in particular during disturbed times when large magnetic storms occurred frequently). Thus the median value was calculated for the period from the start time of the observation to the end of the ERS(m). In the future the subtracting offset value will be corrected by taking into account the secular variation of the base level, though the value is currently determined as a constant.

Figure 11b plots the superposed H component perturbation field data that was observed during the night time (LT = 18–06) at each station: ERS(m) |LT=18–06. The solid thick curve (orange) in Fig. 11b is the Dst value for the same plot interval. This Dst was provided in real-time on the website of the World Data Center for Geomagnetism, Kyoto (http://swdc234.kugi.kyoto-u.ac.jp/dst realtime/). In this figure, Dst was graphically shifted downward so as to avoid overlap with MAGDAS/CPMN data. It is noticed that the nighttime variation of each station was almost aligned with each other and formed a common base magnetic variation. On the other hand, by comparing Fig. 11a and 11b, it can be confirmed that the daytime EEJ component of each station bulged out independently from the base magnetic variation. With this presentation, it is evident that the base magnetic variation ERS(m) |LT=18–06 varies closely with the traditional Dst (Sugiura, 1963). This similarity will be further examined later in this section. "EDst1h" is one-hour average of EDst1m. In Fig. 11c, EDst1h is plotted the green curve. The blue and orange curves in Fig. 11c are 6-h running averages of EDst1h (labeled EDst6h) and the real-time Dst, respectively. Dst is shifted +42 nT to adjust the base level. It is confirmed that the EDst and Dst exhibited the similar temporal variation. It is noticed that EDst6h is less deviated from Dst than EDst1h. Correlation coefficients between EDst6h and Dst, and that between EDst1h and Dst, which were calculated for the 1-month period of December 2006, were 0.93 and 0.88, respectively. It is also found that the correlation coefficient between the low-pass-filtered EDst6h and the low-pass-filtered Dst with the cut-off-period of 2 days was 0.98 is larger than the above-mentioned 0.93.

Figure 11d shows the relative magnetic perturbation of each station, which was calculated by subtracting EDst6h from the H component data. In this calculation, EDst6h was converted to 1-min resolution data by interpolating the original EDst6h through application of the FIR (finite duration impulse response) low-pass interpolating method. It is considered that the positive and negative deviations represent the EEJ and CEJ components, respectively. Uozumi et al. (2008) define those two component as EUS(m) and ELS(m), respectively. For example, when the EU and EL components are derived for the DAV station, those values are expressed as EUDAV(m) and ELDAV(m), respectively. Inspection of these data reveals that the EEJ intensity varies from day to day; moreover, the peaks and dips of each station are not in-phase with other stations. For example, the intensity of EEJ at the DAV station (blue line) and at the ANC station (red line) attained local maxima on Dec. 6 and 8, respectively. The mechanism of the 2-day separation is one of the open questions concerning EEJ. In some cases, it will be necessary to correct the secular variation of a base level to determine EDst6h for properly extracting the EU and EL component.

Jul. 1, 2005 - Mar. 4, 2006

Variable	Peak Period [day]								
(DAV H) - (Dst)	7.5				14.5				35.3
(DAV H)	7.7	9.2	11.2		14.5	17.6	22.5	27.4	
Dst	7.7	9.2	11.2			17.6	22.5	27.4	
Kp		9.2						27.4	
IMF $B_{x,y,z,T}$		9.2		13.7				27.4	
Vsw		9.2		13.0				27.4	
Tsw		9.2		13.0				27.4	
Nsw		9.2	11.2					27.4	35.3
P_D		9.2	11.2					27.4	35.3
ε		9.2					22.5		
F10.7							22.5		35.3

Table 1. Dominant peak periods detected in the power spectrum for various parameters during the period from July 1, 2005 to March 4, 2006.

Uozumi et al.(2008) estimated the power spectrum of the subtracted H component data at DAV; (DAV H) −(Dst) during the period from July 1, 2005 to March 4, 2006. It is recognized that there are at least three dominant peaks at 7.5, 14.5, and 35.3 day (these dominant peaks were visually identified in the figure). Table 1 shows the list of dominant period peaks of various parameters. In the tables, (DAV H) refers to the original (without Dst subtraction) H component data at DAV. IMF (BX , BY , BZ and BT), VSW, TSW, and NSW are the interplanetary magnetic field, solar wind velocity, temperature, and number density, which were observed by the ACE spacecraft. PD and ε are the dynamic pressure and the epsilon-parameter, respectively (Perreault and Akasofu, 1978) calculated by using the ACE solar wind data. F10.7 represents the flux of the solar radio emission at 10.7 cm wavelength. The data of F10.7 was provided at the website of the Herzberg Institute of Astrophysics (http://www.draoofr. hia-iha.nrc-cnrc.gc.ca/icarus/www/archive.html). It is noteworthy that the above-stated dominant period peaks of 7.5 and 14.5 days, which appeared in the spectrum of (DAVH)−(Dst), did not have their roots in the geomagnetic activity indices of Dst and Kp nor any parameters such as IMF, VSW, TSW, NSW, PD, ε, and F10.7, although the peak at 35.3 days was also identified in NSW, PD, and

F10.7. On the other hand, the original H component data contained the same spectrum component as geomagnetic activity indices and solar wind parameters, except 35.3 day.

3.4. Estimation of plasma mass density

The field line resonance (FLR) oscillations in the Earth's magnetosphere are excited by external source waves, and are so-called as ultra low frequency (ULF) waves (cf. Yumoto, 1988). The amplitude of H-component magnetic variations observed at the ground stations reaches a maximum at the resonant point, and that its phase jumps by 180 degrees across the resonant point (see Yumoto, 1985). The eigen-frequency of FLR oscillations is dependent upon the ambient plasma density and the magnetic field intensity in the region of geospace threaded by the field line, and the length of the line of force. The left of Figure 12 shows f-t diagrams obtained at MLB and HOB stations in Australia, phase difference between the two station, and the H-component amplitude ratio of MLB/HOB. The right panel shows the relation among the FLR, eigen-period, length of line of force and the plasma mass density, and the schematic illustration of plasmasphere. When we observe the eigen-frequency of FLR and assume models for the latitude profiles of the magnetic field and the plasma density (with the equatorial density as a free parameter), we can estimate the plasma mass density in the magnetosphere. Therefore, the FLR oscillations are useful for monitoring temporal and spatial variations in the magnetospheric plasma density. By using ground-based network observations, we can identify the FLR phenomena and measure the fundamental field-line eigen-frequency by applying the dual-station H-power ratio method (Baransky et al., 1985) and the cross-phase method (Baransky et al., 1989, Waters et al., 1991), which have been established to identify the FLR properties (Abe et al., 2006, Takasaki, et al., 2006, Maeda N. et al., 2009).

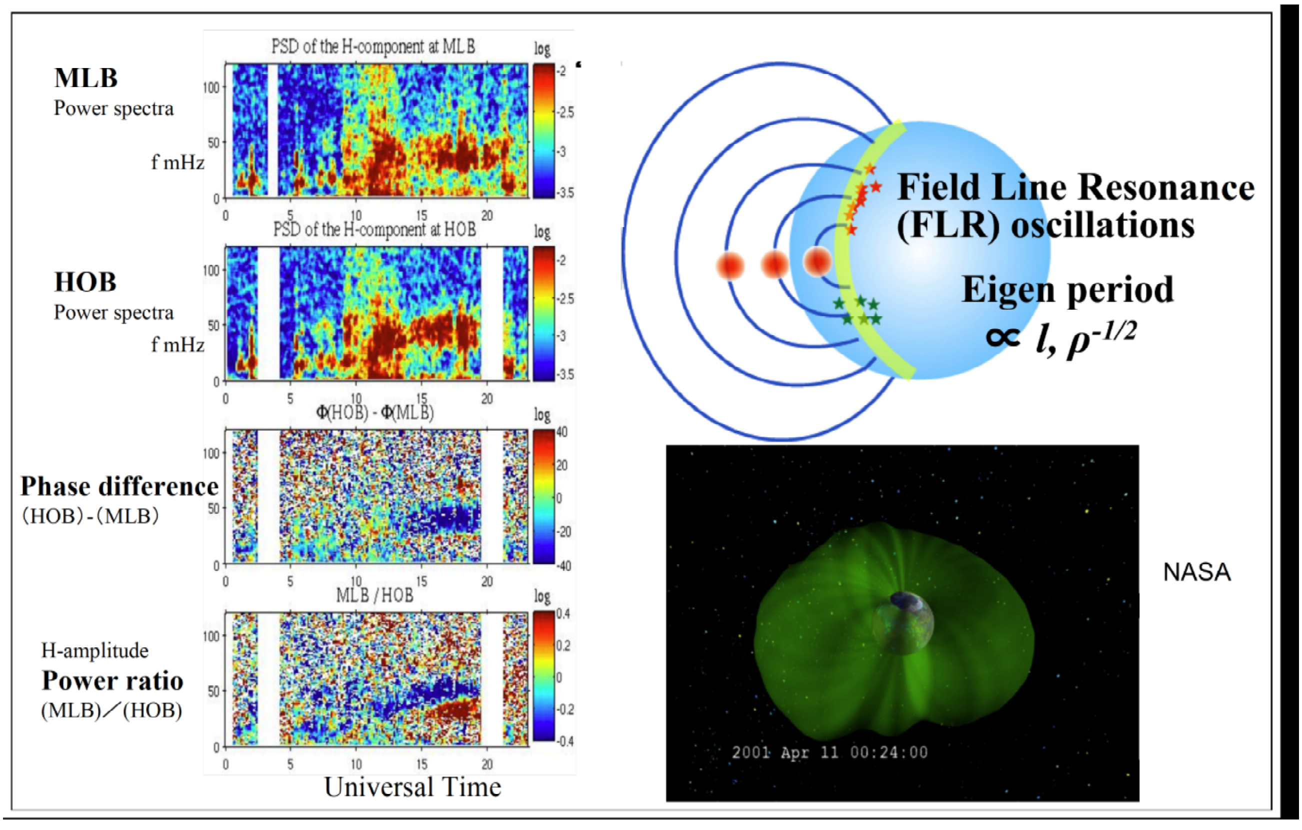

Fig. 12. (left) f-t diagrams of ULF waves observed at MLB and HOB stations in Australia, phase difference between the two station, and the H-component amplitude ratio of MLB/HOB. (right) the relation among the FLR, eigen-period, length of line of force and the plasma mass density, and the schematic illustration of plasmasphere.

By applying the cross-phase method and the amplitude-ratio method to magnetic field data obtained from two ground stations located close to each other, Maeda N. et al. (2009) determined the frequency of the field line resonance (FLR), or the field line eigenfrequency, for the field line running through the midpoint of the two stations. From thus identified FLR frequency they estimated the equatorial plasmamass density (q) by using the T05s magnetospheric field model (Tsyganenkoet al., 2005) and the equation of Singer et al. (1981). They further compared the plasma mass density (q) estimated from magnetometer data at two stations in the CPMN (Circum-pan Pacific Magnetometer Network) chain, Tixie (TIK, geographic coordinates: 71.59°N, 128.78°E, L~ 6:05) and Chokurdakh (CHD, geographic coordinates: 70.62°N, 147.89°E, L~ 5:61), with the plasma electron number density (Ne) observed by the WHISPER (Waves of High frequency Sounder for Probing the Electron density by Relaxation) instrument onboard the Cluster satellites. For the interval of January 1, 2001–December 31, 2005, they have identified 19 events in which the Cluster spacecraft were located on the field line running through the midpoint of TIK and CHD when they observed FLR, and statistically compared the simultaneously observed q and Ne, although the number of events are limited (19). In 15 out of the 19 events the ratio of q to Ne is found to fall into a realistic range. It is also suggested that the contribution of heavy ions tends to increase when the magnetosphere is disturbed.

Takasaki et al. (2006) discussed temporary variations of the plasma mass density by using the two methods during magnetic storm. From ground-based observations at L~1.4 they found a significant decrease in the FLR frequency at during a large magnetic storm as shown in Figure 13. During 28 - 31 October, 2003, a series of coronal mass ejections hit the magnetosphere and triggered two consecutive large storms. Three ground magnetometers at L = 1.32~1.41 recorded field-line resonances (FLRs) during this interval. The FLR frequencies decreased from 0600 LT on 31 October 2003 during in the main phase of the second storm until 12 LT when the recovery phase of this storm began. After the decrease, the FLR frequencies increased to its value before the storm started at 0600 LT on 31 October in a few hours. The measured decrease in FLR frequency might indicate a relative increase in mass density along the field lines during the magnetic storm. On the other hand, the plasma number density in the ionosphere estimated from TEC values was similar in magnitude taken during quiet time. A possible explanation for the increase in mass density would be an outflow of the heavy ions (e.g., O^+) from the ionosphere to the plasmasphere.

Abe et al. (2006) have applied the dual-station H-component power ratio method, which identifies the field-line eigen-frequency, to eleven-months magnetometer data obtained at two ground stations TIK (L=5.98) and CHD (L=5.55) that belong to the Circum-pan Pacific Magnetometer Network (CPMN). As a result, they have identified two patterns in the frequency dependence of the power ratio (TIK/CHD); one is an increase-then-decrease pattern (named Type 1), and the other is a decrease-then-increase pattern (named Type 2). Type 1 is observed where the Alfv´en velocity (V_A) decreases with increasing L, and it has often been reported in literature. In the paper, they mainly studied the Type 2 events w hich have rarely been reported for the area near L=5.7 (midpoint of TIK and CHD); Type 2 is expected to be observed where V_A drastically increases with increasing L. Their statistical analysis shows that the Type 2 events were observed more frequently in the afternoon sector (especially in 15~18 hr LT) than in the morning sector as shown in Figure 14. The geomagnetic condition was usually quiet

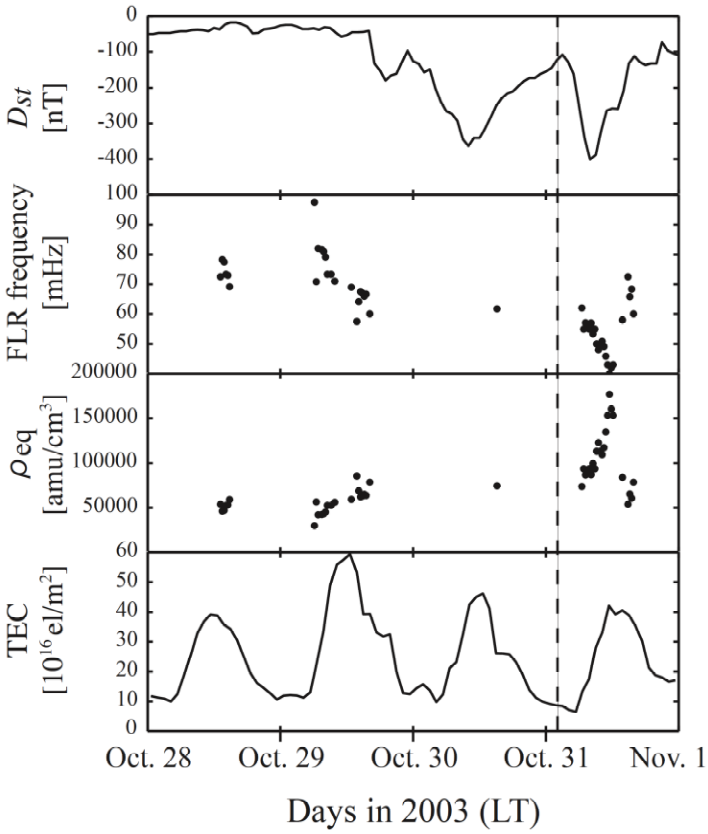

Fig. 13. (From top to bottom) Dst index, FLR frequencies derived from ground observations at L~1.4, ρ_{eq} estimated from data in the second panel, and the total electron content (TEC). The dashed vertical line marks the beginning of the second magnetic storm (Takasaki et al., 2006).

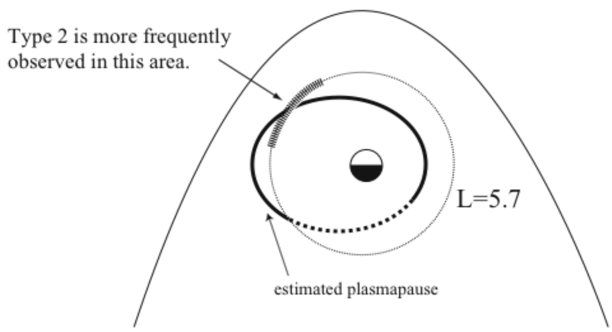

Fig. 14. Schematic picture of the plasmapause location (view from above the north ple). The place where mant Type 2 FLR events were observed is shown by the thick line, and the estimated plasmapause is shown by the black ellipse (Abe et al., 2006).

when the Type 2 events were observed. These features are consistent with the interpretation that their Type 2 events were observed at the footpoint of the plasmapause layer, as follows. The plasmapause is the only location around L=5.7 where V_A drastically increases with increasing L, leading to Type 2. L of the plasmapause is smaller than 5.7 at all LT during geomagnetically active times (meaning Type 1 at L=5.7) while it is larger than 5.7 only on the late-afternoon sector during quiet times.

3.5. Latitudinal dependence of Pc 3-4 amplitudes along 96° MM and Pi 2 along 210° MM

In order to investigate Pc3-4 magnetic pulsations with periods of 10-45 sec and 45-150 sec, respectively, at equatorial and very low latitudes up to mid latitudes, Takla et al. (2009) analyzed geomagnetic data simultaneously obtained from MAGDAS II African stations for more than three and a half months from 4th of October 2008 up to 22nd of January 2009. During this period they selected 21 Pc3 events for studying the latitudinal dependence of Pc3 amplitude and 25 events in case of Pc4. All of the selected events were in daytime ranging from 6 am up to 6 pm local time. Figure 15 shows latitudinal dependence of Pc 3-4 magnetic pulsations observed at the MAGDAS II stations in the African 96° magnetic meridian.

As shown in Fig. 15, they found that the Pc3 amplitudes showed a peak at low latitudes stations with a depression at the dip equator (represented by Addis Ababa station). While the Pc4 amplitudes showed a peak at dip equator and started to decrease by increasing latitude up to mid latitudes. This decrease of the Pc3 amplitudes at magnetic dip equator may be explained as a result of the ionospheric shielding effect on short-period (10-45 sec) hydro-magnetic wave, while the enhancement of Pc 4 amplitude with 45-150 sec period maybe driven by the enhanced equatorial current at magnetic dip equator. Therefore, they conclude that the equatorial Pc3 is originated from the upstream wave, which is propagating as a magnetosonic mode across the ambient magnetic field into the equatorial ionosphere (cf. Yumoto et al., 1985). On the other hand, the equatorial amplitude enhancement of Pc4 may be explained by the penetration of wave electric field of Pc4 range filed-line resonance oscillation, coupled at higher latitudes with surface wave, into the magnetic equator.

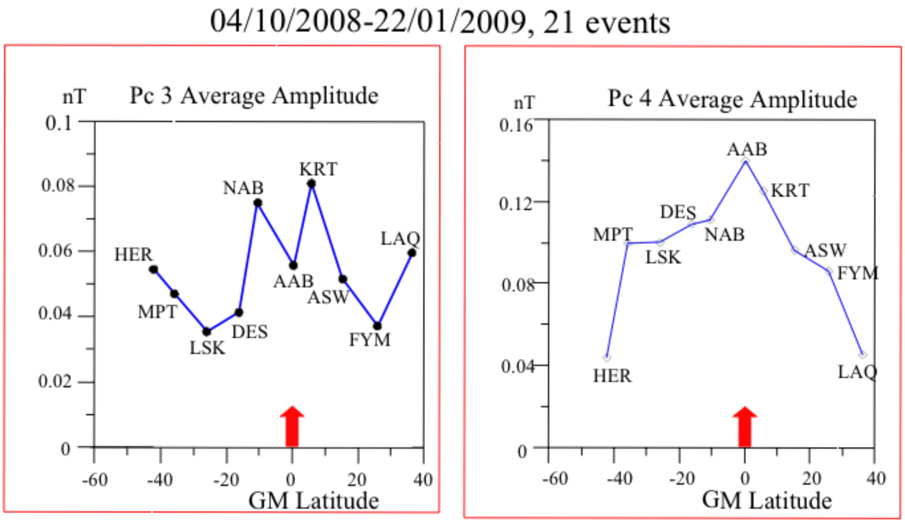

Fig. 15. Latitudinal dependence of equatorial and low-latitude Pc 3-4 amplitude along 96° MM

On the other hand, Pi 2 magnetic pulsations, impulsive hydromagnetic oscillations with a period of 40–150s, occur globally at the onset of magnetospheric substorm expansion phase. From the long term accumulation of the observations, it has been found that Pi 2 pulsations observed on the ground are a superposition of several different components [e.g., Yumoto and the CPMN Group, 2001]. Ground Pi 2 pulsations are mixtures of several components reflecting (1) propagations of fast and shear Alfve´n wave, (2) resonances of plasmaspheric/magnetospheric cavity and magnetic field lines, and (3) transformations to ionospheric current systems. However, it has been unclear how they coupled with each other and how their signals are distributed at different latitudes. The present work is intended to pilot the future possibilities whether we can identify the global system of Pi 2 pulsations by Independent Component Analysis (ICA). Tokunaga et al. (2007) have applied the ICA to the observed CPMN data based on the ICA mode. The dimension of vector x was twenty (i.e., m = 20), the number of source signals was unknown. In this case, they assumed that the observed data was composed of seven independent components and reduced the dimension of the vector to seven via PCA (so the dimension of matrix W become 7 x 20). And then, seven Independent Components (ICs) were calculated by updating the iteration. They made waveforms of ICs estimated by the FastICA. Since the propagation time was ignored in the ICA model, they had to take into account the possibility that these ICs were separated excessively. Thus, they decided to classify these ICs into some groups depending on their waveforms and kurtosis. Kurtosis, which is a classical measure of non-Gaussianity, is defined as $\mathrm{kurt}(x) = E\{x^4\}/[E\{x^2\}] - 3$, whose x is the normalized random variable. kurt(x) becomes 0 if has a Gaussian distribution and positive (negative) if has a super-Gaussian (sub-Gaussian) distribution. Kurtosis of each IC were as follows: IC 1: 19.11, IC 2: 19.26, IC 3: 6.89, IC 4: 3.53, IC 5: 2.80, IC 6: 0.56, IC 7: -0.38. Since the kurtosis of IC 6 and 7 were quite close to 0, each was regarded as noise (especially, IC 7 seem to be strongly affected by periodic noise of ZYK data). Next, IC1, IC2, IC3, IC4 and IC5 were classified into two groups: IC1, IC2 were classified into Group (A), IC3, IC4, IC5 were classified into Group (B).

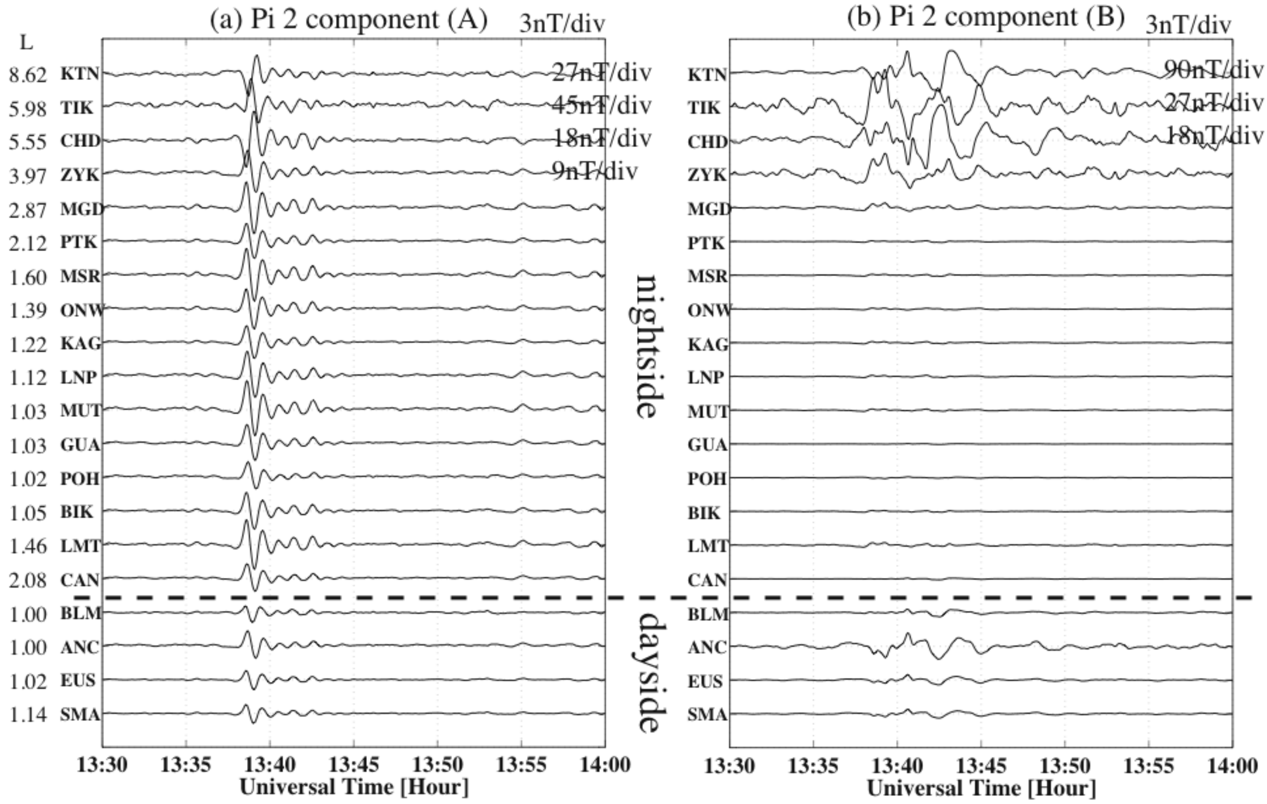

Fig. 16. (a) Separated Pi 2 component (A) plotted as a linear combination of IC 1 and IC 2. (b) Separated Pi 2 component (B) plotted as a linear combination of IC 3, 4 and 5. (see Tokunaga et al., 2007)

Tokunaga et al. (2007) have successfully decomposed an isolated Pi 2 event on a quiet day observed at the CPMN stations into two components. One was the global oscillation that occurs from nightside high to equatorial latitudes with the common waveform and has an amplitude maximum at nightside high latitude. Another component was localized at nightside high latitudes. Its amplitudes were quite weak at low latitudes, but were enhanced near dayside dip equator. Figures 16a and 16b show Pi 2 components plotted as a linear combination of ICs classified into group (A) and group (B), respectively. They call them Pi 2 component (A) and Pi 2 component (B) in the following descriptions. As shown in Figure 16a, it was found that Pi 2 component (A) distributed globally at nightside high, low and equatorial latitudes. Although they seemed to be coherent of each other at low latitudes, there was a phase reversal between CHD and ZYK. In addition, it is recognized that there is a phase shift between TIK and CHD. While, as shown in Figure 16b, it was found that Pi 2 component (B) locally distributed mainly at nightside high latitudes. Although they were hardly seen at nightside low latitudes, at ANC, which was located near dayside dip equator, there was the variation whose waveform was similar to those at KTN. In addition, there was no phase lag between the two stations. As shown in Figure16a, the amplitudes of Pi 2 component (A) were largest at TIK and one order larger. They decreased exponentially from nightside higher to lower latitudes but were enhanced at ANC, which was located near dayside dip equator

4. Ionospheric electric field observations by FM-CW radar

In order to investigate penetration mechanisms of the ionospheric electric fields from the polar to the equatorial ionosphere, SERC has installed a FM-CW (Frequency Modulated Continuous Wave) radar array at Paratunka, Russia (PTK: Magnetic Latitude = $45:8^{o}$, Magnetic Longitude = $221:6\ ^{o}$, LT = UT + 10.5 hrs), Sasaguri, Japan (SSG: M. Lat. = $23:2\ ^{o}$, M. Lon. = $199:6\ ^{o}$, LT = UT + 9.5 hrs) as shown in Figure 17, and Manila, Philippines (MNL:M. Lat. = $4:19\ ^{o}$, M. Lon. = $192:4\ ^{o}$, LT = UT + 8.5 hrs) (see Ikeda et al., 2010a). The height of dipole antenna is 26 m. HF radio wave of 2~42 MHz is emitted in the vertical direction with 20 w power for ionosonde mode, while radio waves of central frequencies (f_0; 2.5 and 8 MHz) for Doppler mode are emitted during night (09 – 21 UT=18 – 06 LT) and day time, respectively. The speed of sweep frequency and the sampling frequency are 100~1000 kHz/sec and 2000~20,000Hz/sec, respectively. This system can measure the Doppler frequency (Δf) of reflected radio wave from the ionized layer and the height of reflection layer with 10-sec sampling rate (Ikeda et al., 2008, 2010a, and b, Yumoto et al., 2009c). From the observed vertical plasma drift velocity ($v = - c\Delta f/2f_0$), we can deduce east-west component of electric field (**E**) in the ionosphere, i.e. **E**= - **v** x **Bo**, where Bo is the ambient magnetic field at the HF radar stations

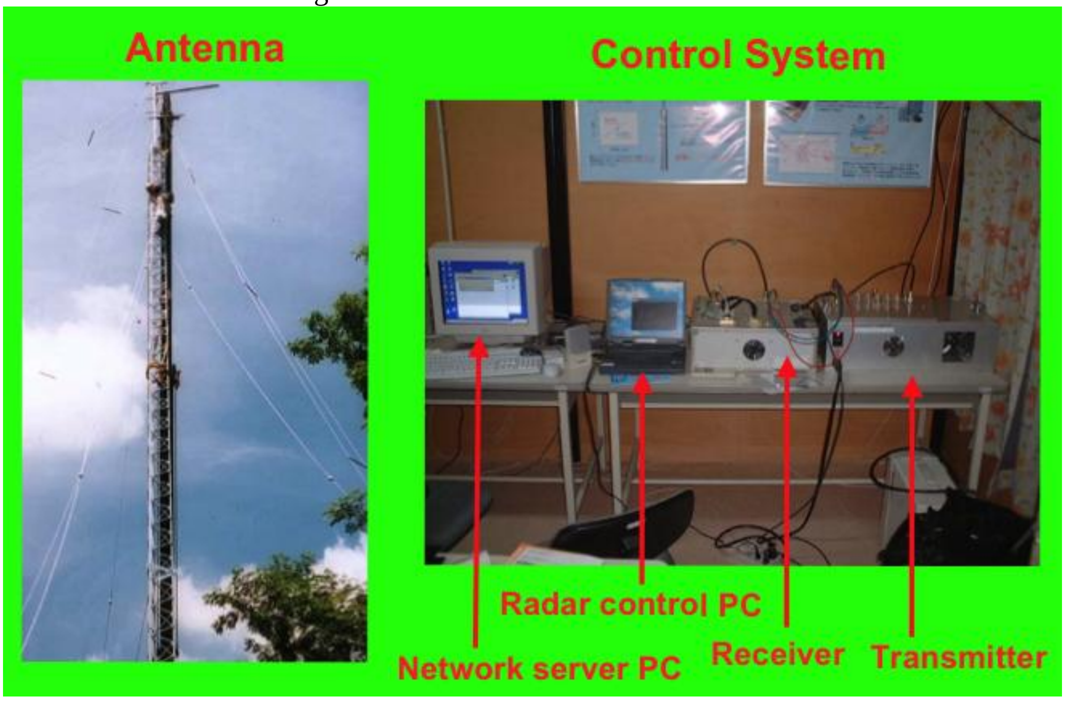

Fig. 17. FM-CW radar system at Sasaguri. 26m dipole antenna (left) and control system including network server, radar control, radio-wave transmitter and receiver (right).

We have performed correlation analysis between ionospheric Doppler data obtained at the FM-CW stations and geomagnetic variations observed at the MAGDAS/CPMN stations, and focus on DP2 type magnetic variations, SC, Pi 2 and Pc 5 magnetic pulsations, which show equatorial enhancements of magnetic field variations at the dip equator. Figure 18 shows H-component DP 2 magnetic variation observed by MAGDAS near ANC during local daytime, and ionospheric DP 2 electric field measured by FM-CW radar at PTK at mid-latitude during nighttime. The equatorial enhancement of dayside DP 2 magnetic variation at ANC can be driven by an ionospheric eastward electric field, while the observed ionospheric westward electric field during the nighttime is synchronized with the DP 2 magnetic variation during daytime.

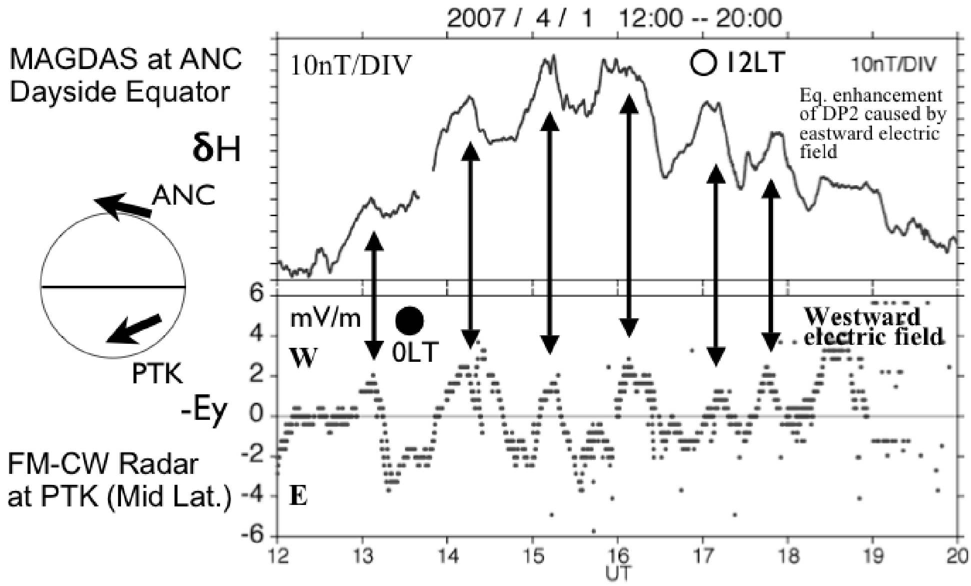

Fig. 18. H-component magnetic DP2 variation observed by MAGDAS at ANC during daytime, and ionospheric electric DP 2 field observed by FM-CW radar at PTK during nighttime on 1 April 2007.

This observation can be interpreted by a scenario in which the IMF Bz variation drives a dawnto-dusk electric field in the solar wind, which penetrates into the polar region and transmits into both the day- and night-sides of the low-latitude ionosphere. It is noteworthy that the H-component DP 2 magnetic variation observed near the magnetic equator during the nighttime indicates roughly in-phase relation with those during daytime, as shown

in Fig. 4. However, it cannot be explained by using the decline in conductivity during the nighttime ionosphere with the ionospheric
DP 2 dawn-to-dusk electric field observed at PTK as shown in Fig 18. A new generation mechanism of DP 2 is needed to understand the globally coherent, DP 2 magnetic variations near the magnetic equator.

The upper panel of Fig. 19 shows SC magnetic variations at KUJ during daytime and at SMA during nighttime, and the associated ionospheric electric field observed at SSG during daytime on 4 November 2003. We can see eastward ionospheric electric field with 0.69mV/m peak-to-peak intensity at SSG and step-like magnetic field variations of about 60 nT amplitude at both KUJ on the dayside and SMA on the nightside. The bottom panel of Fig. 19 shows the SC magnetic variation at KUJ and the ionospheric electric field at SSG observed during nighttime on 21 January 2005. In this case, westward ionospheric electric field of 1.15mV/m peak-to-peak intensity was observed at SSG with step-like magnetic variation of 80 nT at KUJ. Yumoto et al. (2009e) selected 40 SC events that were identified using magnetic data from KUJ and the FM-CW radar data during the period of 2002–2005. At first, they examined step-function-like magnetic changes, and then read the peak-to-peak intensity of the ionospheric electric fields during the SC events. It was found that the ionospheric

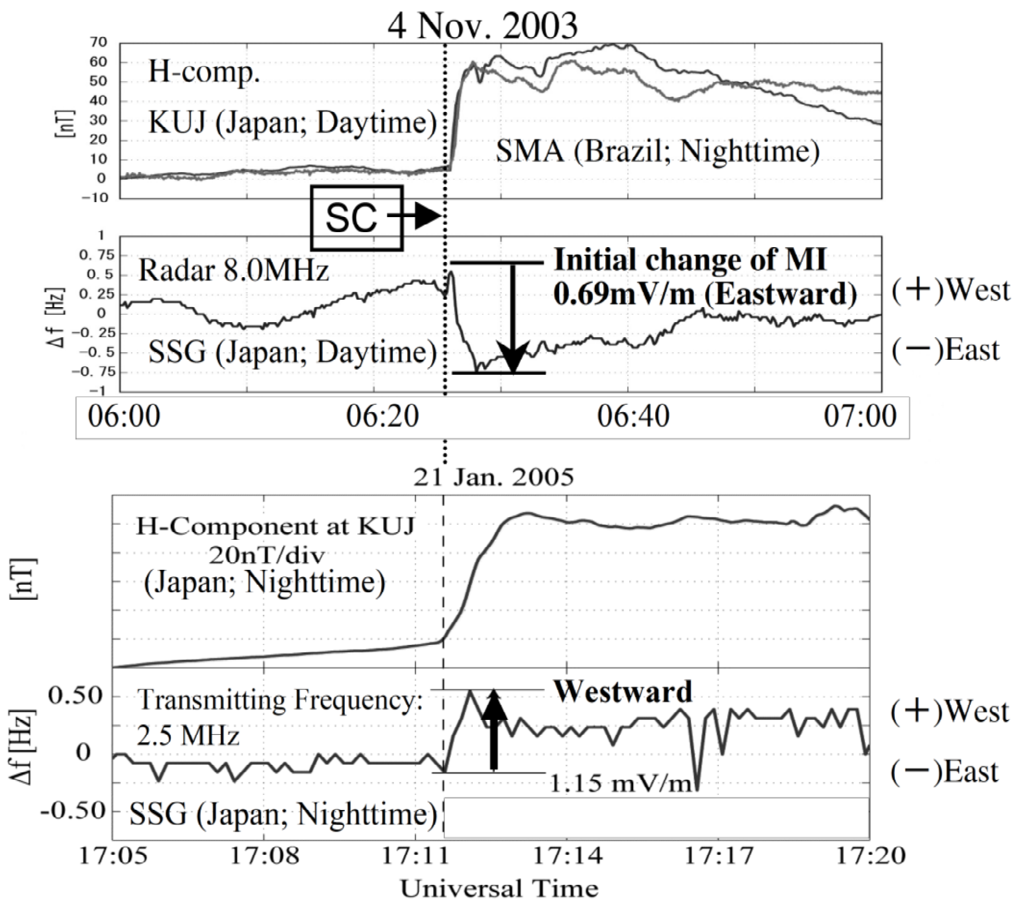

Fig.19. (Upper) Dayside ionospheric electric SC field at SSG with magnetic variations at KUJ during daytime and at SMA during nighttime on 4 Nov. 2003. (Bottom) Nightside ionospheric electric SC field at SSG with magnetic variation at KUJ during nighttime on 21 Jan. 2005.

electric fields denote the direction eastward during daytime (06–20 LT) and westward during the nighttime (17–07 LT). The averaged peak-to-peak intensity of observed electric fields is also found to be 0.5mV/m during the daytime and 1.0mV/m during the nighttime. This daytime and nighttime asymmetries of observed ionospheric electric fields cannot be interpreted using only the penetration model of polar dawn-to-dusk electric field into the day- and night-side lower ionosphere during the SC events. The scale size of changes in the solar wind is too large in comparison to that of the globe; therefore, the day–night asymmetry of the ionospheric electric fields must not be related to the solar-wind conditions. It is needed to study dditional electric field component or a local time-dependence of the penetration efficiency of the polar electric fields into the low-latitude ionosphere. At the onset time of SC preceded by PRI on November 4, 2003, the initial change in the ionosphere was observed simultaneous with the geomagnetic initial change in the accuracy of ±6.4s at 0625UT as shown in Figure 19. Simultaneous observations of the initial changes are not contradictory to the result of the past reports, and approve of the instantaneous penetration of the electric fields to the equatorial latitude. At the same time, it proves the quality of the FM-CW radar as a useful tool for detection of ionospheric electric fields.

Figure 20 shows a nighttime Pi 2 (40-150 seconds) event observed by an FM-CW radar and a MAGDAS magnetometer at PTK on 19 October 2007. During this event, the FM-CW radar observed the altitude of about 250 km (virtual height) at 3.0 MHz. The ground magnetic H and D components obtained at PTK (L = 2.05, LT = UT + 10.5 hrs) and Ashibetsu, Japan (ASB; M. Lat. = 34:7_, M. Lon. = 209:6_, L = 1.48, LT = UT + 9.5 hrs), and Ey at PTK are plotted in Figure 20. The thick lines indicate H components and the thin lines indicate D components. We can see that Pi 2 pulsations were observed simultaneously in H and Ey. They started around 1644 UT and attained their peak around 16:48 UT (see the H component at PTK). The dominant frequency was 15.4 mHz for all waves. The peak-to-peak amplitude of H at PTK, D at PTK, H at ASB, D at ASB, and Ey at PTK are 3.3 nT, 1.4 nT, 2.5 nT, 1.2 nT, and 0.43 mV/m, respectively. The ground magnetic perturbation was dominant at H components rather than at D components. Ikeda et al.(2010b) calculated the cross correlation between Ey at PTK and geomagnetic field data. As a result, the maximum correlation coefficients were 0.95 for Ey-H (PTK), 0.95 for Ey-H (ASB), 0.79 for Ey-D (PTK), 0.72 for Ey-D (ASB). Thus the correlation coefficient of Ey-H is higher than that of Ey-D. In addition, the correlation coefficient of Ey-H (ASB) is higher than that of Ey-H (PTK).Pi 2 pulsations are well known as the signal for the onset of magnetic substorms. Moreover low-latitude Pi 2 pulsations are explained in terms of the plasmaspheric cavity mode, Takahashi et al. (1995).

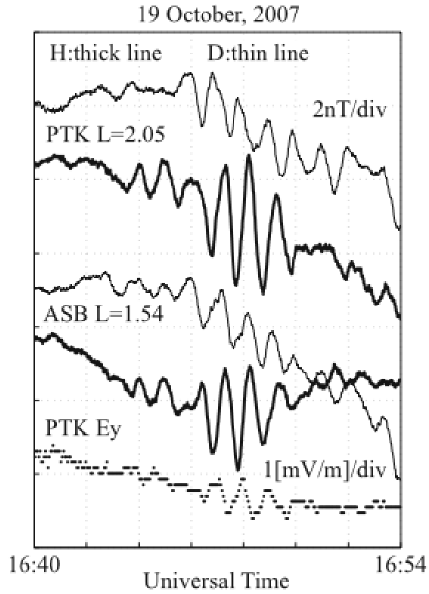

Fig.20. Pi 2 pulsations on 19 October 2007. H and D components at PTK and ASB and Ey at PTK. The thick lines are H components and the thin lines are D components. The transmitting frequency of the FM-CW radar was 3.0 MHz.

The electric field variations (period of about 5 min) associated with Pc5 magnetic pulsations (150-600 sec period) were also observed at the low-latitude ionosphere at Sasaguri (geomagnetic latitude θ=23.2°) during the recovery phase of severe magnetic storm on October 30-31, 2003 as shown in Figure 21. The top and bottom panel show amplitude-time records of H-component magnetic field observed at the MAGDAS/ CPMN station at KUJ (M. Lat. = 23:6°, M. Lon. = 203:2°, LT = UT + 8.7 hrs) and Yap (M. Lat. = 0:42°, M. Lon. = 209:9°, L = 1.00, LT = UT + 9.2 hrs) near the magnetic equator, and the Doppler shifted frequency of HF radio wave measured by FM-CW radar at Sasaguri, respectively, during the period of 00:30-03:30 UT on October 30, 2003. During this event, the FM-CW radar at SAS recorded an altitude of 300 km at 8.0 MHz. The peak-to-peak amplitude of Ey at SAS was about 1.0 mV/m. The magnetic Pc 5 pulsation at YAP was larger than that at KUJ. The peak-to-peak amplitude at YAP was more than 100 nT. This would be due to equatorial enhancement because of the high ionospheric conductivity in the equatorial region. Inspecting the vertical dashed lines in Fig. 21, the peaks of H at YAP almost corresponds with that of Ey at SAS. The positive peaks of Ey correspond with positive peaks of the H. The oscillation of Ey at SAS corresponds with the H at YAP without significant time delay. This result suggests that the ground Pc 5 was excited by the ionospheric electric fields which drive ionospheric currents. The source of Ey for Pc 5 would be caused by the polar dawn-to-dusk

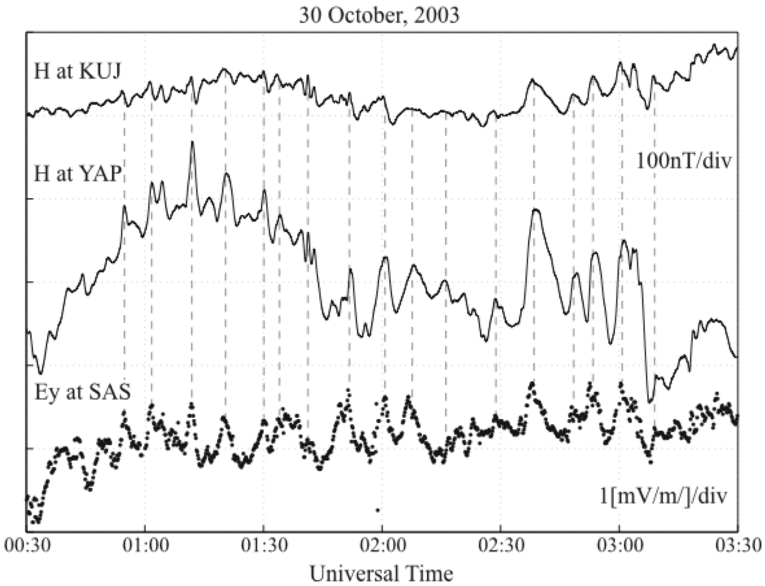

Fig. 21. Amplitude-time records of H-component magnetic field observed at the CPMN station at Yap near the magnetic equator (top), and the Doppler shifted frequency of HF radio wave measured by FM-CW radar at Sasaguri (bottom) during the period of 00:30-03:30 UT on October 30, 2003.

electric fields which are excited by the DP 2 type current system (see, Motoba et al., 2004). This is the evidence of Pc5 magnetic pulsations produced by DP2-type current system in the low latitude ionosphere. In this case, the phase delay of geomagnetic variations was found to be about 10-40 second to the ionospheric variations. We can not ignore the self-inductance effect of enhanced ionospheric current caused by the Cowling conductivity to understand the phase delay of geomagnetic variations observed at the dip equator in daytime (Shinohara et al., 1997).

5. Summary and Conclusion

MAGDAS/CPMN magnetometers were installed at 40 stations along the 210° MM and the magnetic dip equator in 2005 - 2007, including East Asia, Pacific Ocean and Micronesian Islands, and South America and Africa. MAGDAS II system was installed mainly in Africa in 2008. After corrections of the obtained MAGDAS data at SERC, at the first MAGDAS collaborators (the host scientists and others) can access to the SERC server, in which the corrected data are stored, and get 1-min digital data. The corrected 1-sec data will be open for the collaborations with the host scientists at the oversea stations and SERC. Kyushu Univ. SERC also provide the corrected MAGDAS data to the scientific community for collaborative works.

By using the MAGDAS/CPMN system, we can conduct the real-time monitoring for space weather study, and modeling of the global 3-dimensional current system and the plasma mass density variations for understanding electromagnetic and plasma environment changes in the geospace, especially, during the solar flare, coronal mass ejection, magnetic storms, and auroral substorms. Using FM-CW radar array, we are also able to investigate how solar-wind electric fields and polar electric fields of DP-2, sc, Pi2, Pc 5 and other disturbances can penetrate into the equatorial ionosphere. In the present paper, we reviewed the recent results obtained by MAGDAS/CPMN and FM-CW radar system; (1) Imaging of global 3-D current system, (2) Annual and semi-annual Sq current variations, (3) A new EE-index and its long-term variation, (4) Estimation of plasma mass density, (5) Latitudinal dependence of Pc 3-4 amplitudes along 96^{o} MM and Pi 2 along 210^{o} MM, and (6) Ionospheric electric field observations by FM-CW radar.

By using newly established observation systems (such as orbiting satellites and ground-based networks), we can now study the universal physical processes in the “heliospace” – from the Sun to the atmospheres of Earth and the other planets, and throughout the interplanetary medium. During IHY (2007-2009), many developing nations were invited to join the space science community by attending IHY workshops (such as the IHY Tokyo Workshop in 2007), hosting ground instrumentation (such as MAGDAS), and hosting regional IHY schools (such as the IHY Africa School in Nigeria in 2008). But this was only the first step. The next logical step is to continue the nurturing of young scientists in these countries by (1) training them how to do scientific observations and how to use the results, (2) internationally exchanging students and young researchers, and (3) organizing international scientific workshops on their behalf. However, to effectively achieve these goals, we believe there must be regular international scientific conferences that (1) cover the entire region from the Sun to the Earth and the other planets and (2) bring into this discussion the scientists and engineers working in developing countries (who have been neglected in the past). Because of the international scope of this agenda, we suggest that the United Nations coordinate these important plans by initiating an appropriate “post-IHY”, i.e., International Space Weather Initiative (ISWI) program.

During the ISWI period (2010-2012), we will conduct coordinated near-earth JAXA satellite (ETS-VIII, QZS) and MAGDAS observations in Siberia, where 10 new MAGDAS magnetometers will be installed near the foot points of the Quasi-Zenith Satellite (QZS) for space weather, and an international collaboration (Asian network) to establish the short-term EQ prediction in southern Sumatra, Indonesia, where 10 ULF-EM(MT) sites will be constructed in 2010 with inter-sensor distance of 100-200 km.

6. Acknowledgements

The PI of MAGDAS/CPMN project, K. Yumoto, SERC, Kyushu University gratefully acknowledges the dedicated work of his staff at SERC and students at Department of Earth and Planetary Sciences, Kyushu University, and all host scientists at the MAGDAS/CPMN stations located around the world. They made the MAGDAS/CPMN Project possible and successful. The PI also gratefully acknowledges the strong support received from key members of the IHY community: Prof. Hans Haubold (United Nations Office for Outer Space Affairs), Dr. Joseph Davila (NASA), Dr. Nat. Gopalswamy (NASA), and Dr. B. Rabiu (MAGDAS Coodinator of Africa). Financial supports were provided by Japan Society for the Promotion of Science (JSPS) as Grant-in-Aid for Overseas Scientific Survey (15253005, 18253005) and for publication of scientific research results (188068). The IHY Organizer in Japan, K. Yumoto (SERC, Kyushu Univ.) would like to thank the following Japanese IHY Coordinators for their tireless efforts and contributions to the IHY Program in Japan: Secretary of Japan IHY, Dr. S. Watari (NICT), Prof. T. Sakurai (Natl. Astron. Obs. of Japan), Prof. M. Kojima (STE Lab., Nagoya Univ.), Prof. K. Shibata (Kwasan/Hida Obs., Kyoto Univ.), Prof. M. Fujimoto (JAXA/ISAS).

References

1. Baransky, L.N., Y. E. Borovkov, M. B. Gokhberg, S. M. Krylov and V. A. Troitskaya, “High resolution method of direct measurement of the magnetic field line eigen-frequencies, Planet. Space Sci., Äi0vol. 24, pp. 1369-1376, 1985.
2. Baransky, L.N., S. P. Belokris, Y. E. Borovkov, M. B. Gokhberg, E. N. Fedorov, and C. A. Green, “Restoration of the meridional structure of geomagnetic pulsation fields from gradient measurements”, Planet. Space Sci.,Äi0vol. 37, p. 859, 1989.
3. Hibberd, F. H. (1981): Day-to-day variability of the Sq geomagnetic field variation. Aust.310 J. Phys., **34**, 81-90.
4. Huang C-S, K. Yumoto, S. Abe and G. Sofka (2008): Low-latitude ionospheric electric and magnetic field disturbances in response to solar wind pressure enhancements, J. Geophys. Res., Vol. **13**, A08314, doi:10.1029/2007JA012940, 2008.
5. Ikeda A., K. Yumoto, M. Shinohara, K. Nozaki, A. Yoshikawa, A. Shinbori (2008): SC-associated Ionospheric Electric Fields at Low Latitude : FM-CW Radar Observation, Memoirs of the Faculty of Sciences, Kyushu University, Series D Earth and Planetary Sciences, Volume XXXII, No. 1, pp.1-6.
6. Ikeda, A., K. Yumoto, M. Shinohara, K. Nozaki, A. Yoshikawa, M.G. Cardinal, B.M. Shevtsov, V.V. Bychknov, Q. M. Sugon, Jr., and D. McNamara (2010a); Ionospheric observation using FM-CW radar array, Advance in Geoscience, in press.
7. Ikeda A., K. Yumoto, T. Uozumi, M. Shinohara, K. Nozaki, A. Yoshikawa, V.V. Bychkov, and B.M. Shevtsov (2010b), The phase relation between Pi 2-associated ionospheric Doppler velocity and magnetic pulsations observed at a mid-latitude MAGDAS station, J. Geophys. Res., Vol. 115, doi10.1029/2009JA014397, pp.1-7.
8. Kitamura, K., Yumoto, K., and the 210^{o} MM Magnetic Observation Group. (1998) Nothern/southern hemisphere asymmetry of sc/si in the nighttime sector, Proc. NIPR Symp., Upper Atmos. Phys.,12, 108-114.
9. Kohta, H., T. Uozumi, K. Kitamura, A. Yoshikawa, M. Shinohara, MAGDAS group and K. Yumoto, “MAGDAS preliminary report: real-time monitoring of global current structure”, Abstract of 118th SGEPSS Fall Meeting, held at Kyoto Univ., on September 28, 2005, B41-08.
10. Maeda, G., K. Yumoto and the MAGDAS Group (2009); Progress report on the deployment of MAGDAS, Earth Moon Planet, doi 10.1007/s11038-008-9284-5, vol.104, pp.271-275.
11. Maeda, N., S. Takasaki, H. Kawano, S. Ohtani, P. M. E. Decreau, J. G.Trotignon, S. I. Solovyev, D. G. Baishev, and K. Yumoto (2009), Simultaneous observations of the plasma density on the same field line by the CPMN ground magnetometers and the Cluster satellites, *Advances in Space Research* (J. Adv. Space Res.), **43**, doi:10.1016/j.asr.2008.04.016, p.265-272.
12. Matsushita, S., and Campbell, W.H. (1967), Physics of Geomagnetic Phenomena, 2 volumes(International Geophysics Series, Vol. 11), Academic Press, New York and London.
13. Motoba, T., T. Kikuchi, T. F. Shibata, and K. Yumoto (2004), HF Doppler oscillations in the low-latitude ionosphere coherent with equatorial long-period geomagnetic field oscillations, J. Geophys. Res., 109, A06214, doi:10.1029/2004JA010442.
14. Otadoy, R.E.S., D. McNamara, K. Yumoto, and MAGDAS group (2009); Proposal to use theMAGnetic Acquisition System(MAGDAS) of the Circum Pan-Pacific Magnetometer Network (CPMN) to study the equatorial electrojet: A Philippine contribution to the International Heliophysical Year, *Earth Moon Planet*, doi 10.1007/s11038-008-9271-x., vol. 104, pp. 167-172.
15. Rabiu, A.B., I.A. Adimula, K. Yumoto, J.O. Adeniyi, G. Maeda, and MAGDAS/CPMN project group (2009a); Preliminary results from the magnetic field measurements using MAGDAS at Ilorin, Nigeria, *Earth Moon Planet*, doi 10.1007/s11038-008-9290-7, vol. 104, pp. 173-179.
16. Rabiu A.B., Yumoto K., Shiokawa K., and Fujimoto A. (2009b); Equatorial electrojrt parameters along 210◦ magnetic meridian using a thick shell model format: Preliminary results, *Proc. of the Workshop on Equatorial Atmosphere*, Research Institute for Sustainable Humanosphere, Kyoto University, 159-166.
17. Rastogi, R. G., S. Alex and A. Patil (1994): Seasonal variations of geomagnetic D, H and Z fields at low latitudes. J. Geomag. Geoelectr., **46**, 115-126.
18. Rastogi R.G. and K. Yumoto (2007): Equatorial electrojet in the East Brazil anomaly region, Earth Planet Space, 59, No.2, 103-106.
19. Rastogi R.G., H. Chandra, M.E. James, Kentarou Kitamura and K. Yumoto (2008): Characteristics of the Equatorial Electrojet current in Central South America, Earth Planets Space, **60**, 623-632.
20. Richmond, A. D. and J. P. Thayer, “Ionospheric electro-dynamics: A Tutorial”, in Magnetospheric Current Systems, S.-I. Ohtani et al., Eds. AGU, Washington, DC, 2000, p. 131-155.
21. Sastri J.H., Yumoto K., Rao J.V., and Ikeda A (2008): Summer-winter hemisphere asymmetry of the preliminary reverse impulse of geomagnetic storm sudden commencements at midlatitudes: J. Geophys. Res., Vol.113, A05302, 2007JA012968.
22. Shinohara, M., K. Yumoto, A. Yoshikawa, O. Saka, S. I. Solovyev, E. F. Vershinin, N. B. Trivedi, J. M. Da Costa and the 210°MM Magnetic Observation Group, “Wave characteristics of daytime and nighttime Pi 2 pulsations at the equatorial and low latitudes”, Geophys. Res. Lett., Äi0vol. 24, pp. 2279-2282, 1997.
23. Singer,H.J., Southwood, D.J., Walker, R.J., and M.G. Kivelson (1981); M.G. Alfven wave resonances in a realistic magnetospheric magnetic field geometry, J. Geophys. Res. 86 (A6) 4589–4596.

24. Sugiura, M., Hourly values of equatorial Dst for the IGY, Goddard Space Flight Center, Greenbelt, Maryland, NASA Rept., X-611-63-131, June, 1963.
25. Takahashi, K., S.-I. Ohtani, and B. J. Anderson (1995), Statistical analysis of Pi2 pulsation observed by the AMPTE CCE spacecraft in the inner magnetosphere, J. Geophys. Res.,100, 21,929-21,941.
26. Takla E. M., K. Yumoto, S. Abe, A. Fujimoto, A. Ikeda, T. Tokunaga, Y. Yamazaki, T.Uozumi, M. G. Cardinal, A. Mahrous, G. Mengistu, T. Afullo, A. Macamo, L. Joao, N.Mwiinga, C. Uiso, P. Baki, C. Kianji, K. Badi, S. Malinga, A. Meloni and E. Ghamry (2009); Preliminary Results of Latitudinal Dependence of Pc3-ˋ 4 Amplitudes at 96º MM Stations in Africa, Submitted to J. Atmos. Solar-Terres. Phys.
27. Takasaki, S., H. Kawano, Y. Tanaka, A. Yoshikawa, M. Seto, M. Iijima, Y. Obana, N. Sato and K. Yumoto (2006); A significant mass density increase during a large magnetic storm in October 2003 obtained by ground-based ULF observations at L < 1.4, Earth Planets Space, **58**, 617-622.
28. Tanaka Y-M., Yumoto K., Yoshikawa A., Itonaga M., Shinohara M., Takasaki S. and Fraser B.J. (2007): Horizontal amplitude and phase structure of low-latitude Pc3 pulsations around the dawn terminator: J. Geophys. Res. 112(A11): A11308.
29. Tokunaga, T., H. Kohta, A. Yoshikawa, T. Uozumi, and K. Yumoto (2007); Global features of Pi 2 pulsations obtained by Independent Component Analysis, Geophys. Res. Lrtt., Vol. 34,L14106, doi:10.1029/2007GL030174.
30. Tsyganenko, N.A., and M.I., Sitnov (2005); Modeling the dynamics of the inner magnetosphere during strong geomagnetic storms, J. Geophys. Res. 110, A03208.
31. United Nations, New York, (2006) Putting the "I" in the IHY, Comprehensive overview on theworld-wide organization of the International Heliophysical Year 2007.
32. Uozumi, T., H. Kawano, A. Yoshikawa, M. Itonag, and K. Yumoto (2007); Pi 2 source region in the magnetosphere deduced from CPMN data, Planet. Space Sci., 55, 849-857, doi:10.1016/j.pss. 2006.03.01.
33. Uozumi, T., K. Yumoto, K. Kitamura, S. Abe, Y. Kakinami, M. Shinohara, A. Yoshikawa, H. Kawano, T. Ueno, T. Tokunaga, D. McNamara, J. K. Ishituka, S.L.G. Dutra, B. Damtie, V. Doumbia, O. Obrou, A.B. Rabiu, I.A. Adimula, M. Othman, M. Fairos, R.E.S. Otadoy, and the MAGDAS Group (2008): A new index to monitor temporal and long-term variations of the Equatorial Electrojet by MAGDAS/CPMN real-time data: EE-Index, *Earth Planets Space*, **60**, 785-790.
34. Uozumi, T., Yumoto, K., Kitamura, K., Abe, S., Omoto, T., and MAGDAS Group,(2009a); A Calibration Technique for Temperature Drift of MAGDAS Magnetometer Data. *Memoirs of the Faculty of Sciences, Kyushu University, Series D, Earth and Planetary Sciences,* **32(2),** 95-104.
35. Uozumi, T., S. Abe, K. Kitamura, T. Tokunaga, A. Yoshikawa, H. Kawano, R. Marshall, R.J. Morris, B.M. Shevtsov, S.I. Solovyev, D.J. McNamara, K. Liou, S. Ohtani, M. Itonaga, and K. Yumoto (2009b), Propagation characteristics of Pi 2 pulsations observed at high- and low-latitude MAGDAS/CPMN stations: A statistical study, J. Geophys. Res., 114, A11207, 1-16.
36. Waters, C.L., F. W. Menk, and B. J. Fraser, "The resonance structure of low latitude Pc3 geomagnetic pulsations", Geophys. Res. Lett., (1991); vol. 18, pp. 17547-17551.
37. Yamazaki, Y., K. Yumoto, A. Yoshikawa, S. Watari, and H. Utada (2009a); Characteristics of counter-Sq SFE at the Dip equator1 (SFE*) observed by CPMN stations, J. Geophys. Res., vol.114, A05306, doi:10.1029/2009JA014124, pp. 1-5.
38. Yamazaki, Y., K. Yumoto, T. Uozumi, A. Yoshikawa, and M.G. Cardinal (2009b); Equivalent current systems for the annual and semi-annual Sq variations observed along the 210o MM CPMN stations, J. Geophys. Res., Vol. 114, A12320, doi:10.1029/2009JA014638, pp. 1-9.
39. Yoshikawa, A., Nakata, H., Nakamizo A., Uozumi, T., Itonaga, T., and Yumoto, K., (2009); A new magnetosphere-ionosphere coupling scheme for temporal and global magnetospheric MHD simulations. *Memoirs of the Faculty of Sciences, Kyushu University, Series D, Earth and Planetary Sciences,* **32(2),** 87-94.
40. Yumoto, K. (1985); Characteristics of localized resonance coupling oscillations of the slow magnetosonic wave in non-uniform plasma, Planet._Space_Sci., 33, 1029-1036.
41. Yumoto, K. (1988); External and internal sources of low-frequency MHD waves in the magnetosphere --- A review, J._Geomag._Geoelectr., 40, 293-311.
42. Yumoto, K., and the 210^o MM Magnetic Observation Group (1996a); The STEP 210^o magnetic meridian network project, J. Geomag. Geoelectr., 48, 1297-1309.
43. Yumoto, K., H. Matsuoka, H. Osaki, K. Shiokawa, Y. Tanaka, T.-I. Kitamura, H. Tachihara, M. Shinohara, S.I. Solovyev, G.A. Makarov, E.F. Vershinin, A.V. Buzevich, S.L. Manurung, Obay Sobari, Mamat Ruhimat, Sukamadradjat, R.J. Morris, B.J. Fraser, F.W. Menk, K.J.W. Lynn, D.G. Cole, J.A. Kennewell, J.V. Olson, and S.-I. Akasofu (1996b); North/south asymmetry of sc/si magnetic variations observed along the 210o magnetic meridian, J. Geomag. Geoelectr., 48, 1333-1340.
44. Yumoto, K, and the CPMN Group (2001); Characteristics of Pi 2 magnetic pulsations observed at the CPMN stations: A review of the STEP results, Earth Planets Space, 53, 981-992.
45. Yumoto, K., and the MAGDAS Group (2006); MAGDAS project and its application for space weather, Solar Influence on the Heliosphere and Earth's Environment: Recent Progress and Prospects, Edited by N. Gopalswamy and A. Bhattacharyya, ISBN-81-87099-40-2, pp. 399-405.

46. Yumoto K. and the MAGDAS Group (2007): Space weather activities at SERC for IHY: MAGDAS: Bull. Astr. Soc. India 35, 511-522
47. Yumoto, K., S. Ikemoto, M.G. Cardinal, M. Hayakawa, K. Hattori, J.Y. Liu , S. Saroso, Ruhimat M., M. Husni , D. Widarto, E. Ramos., D. McNamara, R.E. Otadoy, G. Yumul, R. Ebora and N. Servando (2009a): A new ULF wave analysis for seismo-electromagnetics using CPMN/MAGDAS data, *Physics and Chemistry of the Earth* (J. Phys. Chem. Earth), doi:10.1016/j.pce.2008.04.005, 34, 360-366.
48. Yumoto, K., and STPP Sub-committee (2009b); International heliophysical year activities in Japan, *Data Science Journal*, Vol. 8, 30 March 2009, pp. S14-S23.
49. Yumoto K., A. Ikeda, M. Shinohara, T. Uozumi, K. Nozaki, S. Watari, K. Kitamura, V. V. Bychkov, and B. M. Shevtsov (2009c): Electric and Magnetic Field Variations at Low and Equatorial Latitudes During Sc, DP2, and Pi2 Events, *Advances in Geosciences*, Vol. **14**, Solar Terrestrial, Eds. Marc Duldig et al., World Sci. Publ. Comp., pp.197-212.
50. Yumoto, K. H. Kawano, and MAGDAS group (2009d); MAGDAS for geospace environment monitoring, , *26th ISTS-ISTS Special Issue of JSASS On-Line Journal*, *Trans. JSASS Space Technology Japan*, Vol.7, No. ists26, pp. Tr_2-Tr_2_4.
51. Yumoto, K., G. Maeda, S. Abe, T. Uozumi, A. Fujimoto, A. Ikeda, T. Tokunaga, Y. Yamazaki, T. Ueno, Y. Hitayama, B. Rabiu, C.B.S. Uiso, P. Baki, K.M. Badi, L. B. Kolawole, T. Afullo, A. Macamo, H. Mweene, and MAGDAS/CPMN Group (2009e); Progress report on the global deployment of MAGDAS, *Sun and Geosphere*, in press.

ПРОЯВЛЕНИЕ МАГНИТО-ОРИЕНТИРОВАННЫХ ИОНОСФЕРНЫХ ПЛАЗМЕННЫХ ВОЗМУЩЕНИЙ НА СРЕДНИХ ШИРОТАХ
MANIFESTATION OF FIELD-ANGLED IONOSPHERE PLASMA DISTURBANCES AT MID-LATITUDE

Э.Л. Афраймович, Э.И. Астафьева, Е.А. Косогоров, Ю.В. Ясюкевич
Институт Солнечно-Земной Физики СО РАН, yasukevich@iszf.irk.ru;

Using technique of magnetic zenith scanning by GPS rays it was shown that unusual northward isolated ionosphere irregularities registered on 5th October 2001 above California are manifestation of field-angled plasma disturbances (FAD). FADs are characterized by positive deviation of the total electron content (TEC) value up to 4 TECU (10^{16} el/m^2). Corresponding TEC variations are isolated impulses with duration of ~40 min. We estimate the influence of such irregularities on differential GPS. Some problems connected with radio signal parameters change may arise when up-to-date very long base interferometers operate, for example, LOFAR or SKA.

1. Введение

Крупномасштабным ионосферным неоднородностям, вытянутым по магнитному полю посвящено множество работ. В литературе рассматривается два типа таких неоднородностей – баблы (bubbles, пузыри) и блобы (blobs) [1-5]. Однако в большинстве работ данные о пространственной геометрии магнитоориентированных неоднородностей (МОН) отсутствуют. Для примера, авторы [1] установили, что их наблюдения представляют проявление бабла используя только следующие критерии: время появления (после заката), наличие фазовых сбоев, уменьшение полного электронного содержания (ПЭС) и плотности электронной концентрации на спутнике DMSP. Однако упомянутые выше критерии недостаточны для идентификации пузыря. Необходимо получить более прямое доказательство вытянутости структуры вдоль магнитной силовой линии (как, например, в работе [2]).

Основное число работ по исследованию баблов и блобов было осуществлено на основе непосредственных измерений электронной концентрации. Только в отдельных работах наряду с измерениями электронной концентрации привлечены измерения ПЭС [1, 2]. Целью настоящей работы является описание метода GPS детектирования среднеширотных магнитоориентированных возмущений и неоднородностей и оценка их влияния на радиотехнические системы на примере необычного явления, имевшего место 5 октября 2001 г. над Калифорнией [6].

2. Метод детектирования среднеширотных магнитоориентированных неоднородностей

Если изолированная неоднородность вытянута вдоль магнитной силовой линии, то при пересечении ее лучами «спутник-приемник» под разными углами мы должны увидеть следующую картину: при приближении луча к области магнитного зенита (т.е. когда луч параллелен магнитному полю) ПЭС будет возрастать (убывать для баблов). При этом мы считаем, что наклонение магнитного поля с высотой меняется достаточно слабо (по крайней мере, на высотах, вносящих определяющий вклад в вариации ПЭС) и линия магнитного поля практически прямая. Тогда во временной области при прохождении области магнитного зенита мы будем видеть «горб» ПЭС.

Стандартный метод GPS позволяет детектировать волновые возмущения на основе фазовых